

AUS Repository

Using a Cavitation Model to Represent the Acoustic Release Kinetics from Folated Micelles

Item Type	Thesis
Authors	Tanbour, Rafeeq Kamal
Download date	2026-05-20 16:57:08
Link to Item	http://hdl.handle.net/11073/7730

USING A CAVITATION MODEL TO REPRESENT
THE ACOUSTIC RELEASE KINETICS
FROM FOLATED MICELLES

by
Rafeeq Kamal Tanbour

A Thesis Presented to the Faculty of the
American University of Sharjah
College of Engineering
in Partial Fulfillment
of the Requirements
for the Degree of

Master of Science in
Chemical Engineering

Sharjah, United Arab Emirates

December 2014

Approval Signature

We, the undersigned, approve the Master's Thesis of Rafeeq Tanbour.

Thesis Title: Using a Cavitation Model to Represent the Acoustic Release Kinetics from Folated Micelles.

Signature

Date of Signature
(dd/mm/yyyy)

Dr. Ghaleb Hussein
Professor
Department of Chemical Engineering
Thesis Advisor

Dr. Paul Nancarrow
Assistant Professor
Department of Chemical Engineering
Thesis Committee Member

Dr. Ana Martins
Visiting Scholar
Department of Chemical Engineering
External Thesis Committee Member

Dr. Naif Darwish
Head, Department of Chemical Engineering

Dr. Mohamed El-Tarhuni
Associate Dean, College of Engineering

Dr. Leland Blank
Dean, College of Engineering

Dr. Khaled Assaleh
Director of Graduate Studies

Acknowledgements

In the name of Allah, the source of all knowledge, nothing could have ever been accomplished or come to existence without Allah's help.

I would like to express my appreciation to my advisor, Dr. Ghaleb Husseini for his great ideas, patience and support throughout my progress, Dr. Ana Martins for her help, patience, and valuable support during the research period, and Dr. Paul Nancarrow for his support and help during the working time.

I would also like to thank my colleagues, Eng. Mohamed Elkhodairy and Eng. Hesham Jamal for their valuable help and suggestions.

Abstract

Anti-neoplastic drugs used for cancer treatment have various damaging effects on healthy cells, leading to several side effects in patients undergoing chemotherapy. The encapsulation of these agents in nanoparticles, such as micelles, reduces their adverse effects on healthy tissues in the body, thus decreasing the side effects of conventional chemotherapy. The aim of this work is to develop a MATLAB program to measure the kinetics of drug release from targeted and non-targeted micelles, triggered by the use of ultrasound, followed by re-encapsulation of the drug in the micelles once the stimulus has been turned off. This program allows the determination of three constants α , β and λ that define the release and re-encapsulation behavior in our drug delivery system. After the simulation was done through the MATLAB program, the results showed that drug release is proportional to increasing power density, as evidenced by the correlation between the *alpha* parameter and power density. Additionally, the re-assembly behavior, quantified by the *beta* parameter also increased as the power density increases. The third parameter, *lambda*, which is associated with the initial phase of the release process, showed a constant value regardless of the insonation power density. A better understanding of the kinetics involved in this drug delivery system helps in determining the best ultrasound parameters to be used in future *in vitro* experiments.

Search terms: Pluronic®, P105, micelles, Dox, cavitation, folated, cancer.

Table of Contents

Abstract	5
List of Figures	8
List of Tables	10
Nomenclature	11
Chapter 1 : Introduction	12
1.1. Background	12
1.2. Objectives.....	14
1.3. Work Methodology	14
1.4. Thesis Organization.....	14
Chapter 2 : Literature Review	15
2.1. Micelles	15
2.2. Ultrasound	17
2.3. Targeting	20
2.4. <i>In vitro</i> and <i>in vivo</i> work	23
2.4.1. <i>In vitro</i> work	23
2.4.2. <i>In vivo</i> work	28
Chapter 3 : Theoretical Analysis.....	31
Chapter 4 : Data Analysis	36
4.1. Experimental Procedure	36
4.2. Data Denoising and Preparation.....	36
4.3. Data Modeling Using the MATLAB Designed Program.....	40
Chapter 5 : Results and Discussion.....	43
5.1. Modeling	43
5.2. Tukey-Kramer's test and T-test for result analysis	46
Chapter 6 : Conclusion and Recommendation.....	51
6.1. Conclusion.....	51

6.2. Recommendations	52
References.....	53
Appendix.....	60
A. Designed Modeling Program for MATLAB:.....	61
B. Voltage to Power Density conversion	65
C. Result Tables	66
D. Release Data Graphs after Denoising:.....	68
Vita.....	78

List of Figures

Figure 1-1: Different types of nano-sized drug carriers.....	13
Figure 2-1: The structure of a polymeric micelle.	15
Figure 2-2: Ultrasonic exposure chamber.....	18
Figure 2-3: The effect of cavitation events on the release of drugs from polymeric micelles. 19	
Figure 2-4: Phases of drug release from micelles in the presence of US.....	20
Figure 4-1: Non-processed data showing the temporal release for Folated-P105-2.183.....	37
Figure 4-2: Overlaid data showing the temporal % release for Folated-P105-2.183.....	38
Figure 4-3: Denoising using the MATLAB software.	38
Figure 4-4: Average data showing the temporal release for Folated-P105-2.183 (Release part).	39
Figure 4-5: Average data showing the temporal release for Folated-P105-2.183 (Re- encapsulation part).....	39
Figure 4-6: Starting and stop point for the modeling.....	42
Figure 4-7: The modeling results obtained using MATLAB.....	42
Figure 5-1: The relation between power density and the amount of destruction of micelles which is quantified by Alpha.	43
Figure 5-2: The relation between the power density and the Beta parameter which is related to the rate of micellar re-assembly.	44
Figure 5-3: The relation between power density and its effect on the drug re-encapsulation parameter lambda.....	45
Figure D-1: Denoised release data for Folated-P105-1.009.....	68
Figure D-2: Denoised release data for Folated-P105-1.062.....	68
Figure D-3: Denoised release data for Folated-P105-1.030.....	69
Figure D-4: Denoised release data for Folated-P105-1.267.....	69
Figure D-5: Denoised release data for Folated-P105-2.183.....	70
Figure D-6: Denoised release data for Folated-P105-2.389.....	70
Figure D-7: Denoised release data for Folated-P105-2.546.....	71
Figure D-8: Denoised Release data for Folated-P105-3.540.	71
Figure D-9: Denoised release data for Folated-P105-5.013.....	72

Figure D-10: Denoised release data for Folated-P105-5.432.....	72
Figure D-11: Denoised release data for Folated-P105-5.914.....	73
Figure D-12: Denoised release data for P105-1.030.....	73
Figure D-13: Denoised release data for P105-1.267.....	74
Figure D-14: Denoised release data for P105-2.183.....	74
Figure D-15: Denoised release data for P105-2.389.....	75
Figure D-16: Denoised release data for P105-2.546.....	75
Figure D-17: Denoised release data for P105-3.540.....	76
Figure D-18: Denoised release data for P105-5.013.....	76
Figure D-19: Denoised release data for P105-5.432.....	77
Figure D-20: Denoised release data for P105-5.914.....	77

List of Tables

Table 4-1: Initialization values for the parameters used for the modeling process.....	41
Table 5-1: Tukey Kramer's test results for <i>Alpha</i> Folated-P105.	47
Table 5-2: Tukey Kramer's test results for <i>Beta</i> Folated-P105.	47
Table 5-3: Tukey Kramer's test results for <i>Lambda</i> Folated-P105.....	48
Table 5-4: Tukey Kramer's test results for <i>Alpha</i> P105.	49
Table 5-5: Tukey Kramer's test results for <i>Beta</i> P105.....	49
Table 5-6: Tukey Kramer's test results for <i>Lambda</i> P105.....	50
Table 5-7: T-test for the parameters in order to get the P-values.....	50
Table A-1: Script Part for the MATLAB Program.	61
Table A-2: Function Part for the MATLAB Program.	63
Table B-1: Voltage to Power Density conversion, and number of replicates for all points.....	65
Table C-1: <i>Alpha</i> (for folated and non-folated micelles).....	66
Table C-2: <i>Beta</i> for folated and non-folated micelles.....	66
Table C-3: <i>Lambda</i> (for folated and non-folated micelles)	67

Nomenclature

CMC	Critical micellar concentration
DDS	Drug delivery systems
Dox	Doxorubicin
EPR	Enhanced permeation and retention
Foliated-P105	Foliated Pluronic P105 micelles
Foliated-P105 (P105)-x	Foliated (or non-Foliated) Pluronic P105 micelles actuated by US with a power density of x
PBS	Phosphate buffered saline
PEO	Polyethylene oxide
PPO	Polypropylene oxide
P105	Pluronic (non-Foliated) P105 micelles
US	Ultrasound

Chapter 1 : Introduction

1.1. Background

In the human body, cells are continuously regenerating and getting replaced in a cycle where older cells die because of a genetic program that defines their life cycle. Once the period over which the cell is programmed to live is over, it gets replaced by new cells which were produced as a result of a process known as cell division. This process happens normally in the body, and its timing depends on the type of the cells (e.g. the epithelial layer in skin should be replaced every 10 days). The cell cycle is controlled at several levels, including at the gene level. Genes are subjected to mutation processes and, in case of a mutation in gene or genes related to cell cycle regulation, the cell division and tissue growth may be impaired and lead to the abnormal growth of cells, originating tumors in tissues and organs [1, 2]. Cancer is a type of tumor which grows unconfined and may spread to several other tissues and organs.

Research in cancer treatment has been the interest of many medical organizations due to it being the leading cause of death in Europe and North America, while being the second leading cause of death in the less developed countries, especially in Africa [3, 4]. The treatment of cancer usually involves subjecting the patient to a chemical treatment, termed chemotherapy, which usually requires different sessions and doses. Although chemotherapy may be effective in cancer treatment, it has unwanted effects on healthy cells and organs. Hence, scientists are searching for other methods in drug delivery to decrease its unwanted effects, without affecting its efficacy in killing cancer cells [5-7].

The science of nano- and micro-technology has been widely used in different branches of science, especially in medicine. Focusing on cancer treatment, it was found that nanoparticles can sequester the chemotherapy drugs inside their core or within their bilayer membrane, depending on the type of carrying vesicles used. Using nanoparticles to encapsulate drugs helps in decreasing the damage caused to healthy cells because it focuses the effect of chemotherapy on the tumor cells by controlling the time when, and space where, the drugs are released [5-8].

There are many types of drug carriers that can be used, including nanospheres, nanocapsules, dendrimers, micelles and liposomes. Different drug delivery carriers are

shown in Figure (1-1). Micelles, the most commonly used vesicles in drug delivery after liposomes, are the focus of this study.

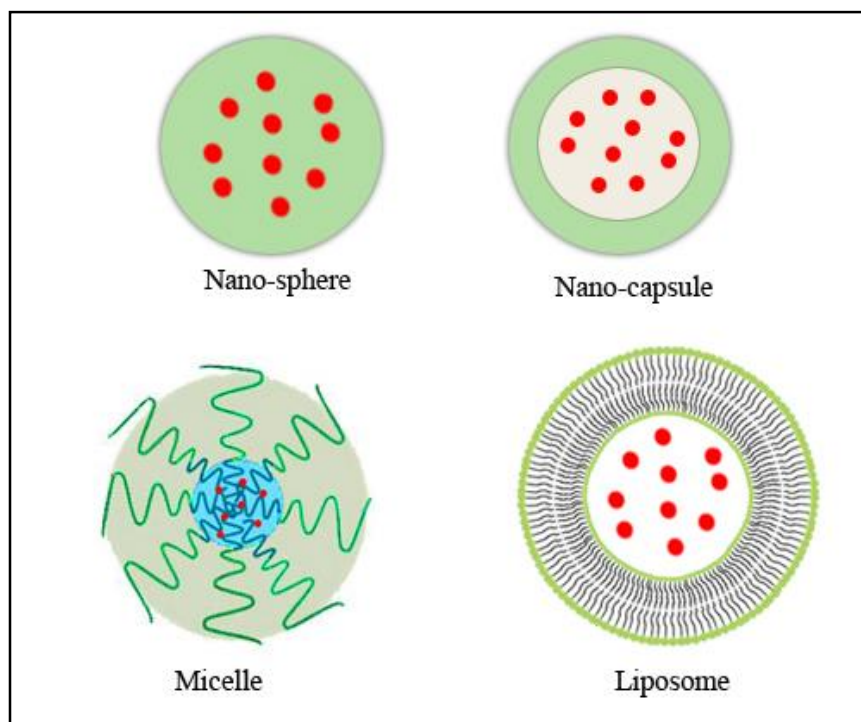


Figure 1-1: Different types of nano-sized drug carriers [6].

There are many types of micelles differing in their composition. The shape and size of these particles are different based on the original material used in their synthesis. Micelles are usually made up of polymeric material that gives them their specific characteristics. Polymeric micelles are amphiphilic blocks of copolymers that self-assemble as core-shell structures. The type of drugs that can be encapsulated inside these carriers depends on the carrier structure, whether the drug is hydrophobic or hydrophilic, as well as on the tumor type [8].

Modifications on drug carrier systems can improve the results of the treatment. The modifications can be done to the carrier itself, for example by adding some targeting moieties to improve their capability to bind to tumor cells. This is called *active targeting*, and one example is the folate moiety, which binds the folate receptor over-expressed on several cancer cells. Additionally, external factors such as ultrasound (US), hyperthermia and magnetic fields, can be used to trigger the drug delivery, a process known as *triggered targeting*. In general, the purpose of these modifications is to target the tumors, while the nano-carriers are referred to as targeted drug delivery carriers [6, 7].

The most common drugs used in chemotherapy belong to the anthracycline family, and Doxorubicin (Dox) is widely used and effective for the treatment of cancer. However, it has several side effects including cardiotoxicity and non-specificity [5, 7].

1.2. Objectives

The main objective of this thesis is to design a computer program using MATLAB in order to fit the experimental release data. Then this program will be used to calculate rate constants for both release and re-encapsulation, for targeted and non-targeted micelles, as a function of power density. Then, a statistical comparison between the different parameters employed in this drug delivery technique will be reported.

1.3. Work Methodology

The aim of this research is the design of a MATLAB program to model the kinetic behavior of release from targeted (Folated) and non-targeted (non-Folated) polymeric micelles, using US as a trigger. The model was originally published in order to calculate the kinetic constants associated with the release and re-encapsulation phenomena associated with drug delivery systems (DDS) [9, 10]. The main concept behind this model is the cavitation phenomenon that generates shock waves piercing the micelles open and releasing the drug.

1.4. Thesis Organization

The structure of this thesis is as follows. First, a detailed literature review on micelles and targeting is presented. Then, the major objectives of the thesis are detailed. The theory of the work, where the model is summarized, is followed by data analysis. In the Results and Discussion section, the results are plotted and analyzed to deduce a general trend, and then discussed in terms of the correlation between each constant and the ultrasound power densities employed in this research. The results comparing the acoustic release kinetics and subsequent re-encapsulation from targeted and non-targeted micelles are also presented followed by the conclusions and future work recommendations.

Chapter 2 : Literature Review

2.1. Micelles

In order to reduce the side effects of conventional chemotherapy drugs on healthy cells, it is important to use an intermediary that sequesters these drugs in a package, and then delivers them to the diseased cells. One of the important carriers currently being studied are micelles formed using the Pluronic® family of tri-block copolymers [11]. The classification of micelles is based on the type of intermolecular forces involved in their formation. In general, there are three types of micelles: amphiphilic micelles with predominance of hydrophobic interactions, polyion complex micelles which have electrostatic interactions, and micelles stemming from metal complexation [12].

Pluronic® micelles are amphiphilic blocks of copolymers that are capable of self-assembling into core-shell structures. They are tri-block copolymers of polyethylene oxide (PEO) and polypropylene oxide (PPO), PEO-PPO-PEO, with a hydrophobic core and a hydrophilic shell, as shown in Figure (2-1). Hence, hydrophobic drugs can be encapsulated inside the core of the micelle to be delivered to the tumor site [11, 13].

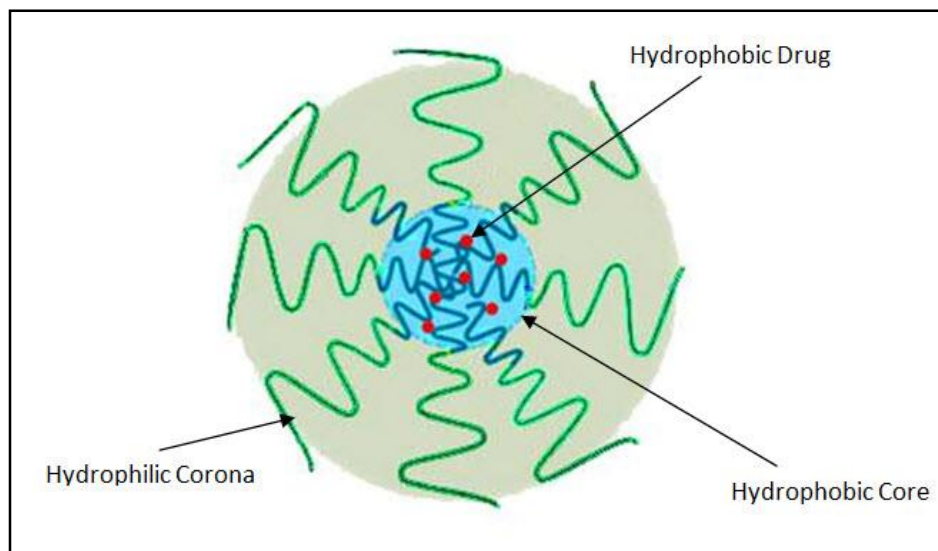


Figure 2-1: The structure of a polymeric micelle [13].

The most common copolymer used in acoustically activated micellar drug delivery is Pluronic® P105. This copolymer chain consists of 37 monomers of PEO and 56 of PPO, with an equal weight fraction of both copolymers. The features that make Pluronic® P105 a good choice over the other copolymeric types are its low

toxicity, quick formation once dissolved in water, and stability above the critical micellar concentration (CMC) due to its hydrophobic core [14]. CMC is defined as the concentration of block copolymer at the time of micelle formation. If the concentration of the block copolymer is below the CMC, the micelles will not form. The stability of these micelles is affected by the CMC, especially when the copolymer is diluted in bodily fluids. At room temperature, the CMC of Pluronic® 105 micelles is close to 1 wt% [15, 16].

The advantages of using micelles as chemotherapy carriers in comparison with other carriers include their inherent size (10 to 200 nm) which helps them to escape renal excretion, while allowing them to extravasate at the tumor site. Additionally, the incorporation of the drugs inside their core is a simple process due to the hydrophobic-hydrophobic interactions between the drug and the PPO core [13, 14, 17, 18]. Furthermore, micelles are easy to prepare, their shelf life is long [15] and, at low concentration, they can sensitize multi-drug resistance (MDR) in cancer cells [19]. One of their main disadvantages, however, is that they disassociate once diluted if the concentration is below their CMC which makes them unstable, so they cannot sequester the drug if their concentration is below a certain threshold [18, 20, 21].

From what was described, it is extremely important to determine the micellar stability in order to know if their structure can release and re-encapsulate the drugs once they reach the intended site. Also, it is very important to study the effect of stability in relation to the rate of elimination of micelles from the body after their release at the tumor site. The stability of micelles can be enhanced by cross-linking their core with a suitable material such as poly(N,N-diethyl acrylamide). This cross-linking will enhance their stability [22-24]. The stability of these micellar structures can be determined using the fluorescent probe diphenyl-1,3,5-hexatriene (DPH) and dynamic light scattering, a technique used to determine the size of particles [11, 25].

The method of incorporating anti-neoplastic agents inside P105 micelles is relatively easy. First, a filtered stock solution of P105 of known concentration is prepared in a phosphate buffered saline (PBS) solution. Subsequently, a solution of the drug is added to the micellar solution, which results in micelles encapsulating the drug at a known concentration [26, 27].

2.2. Ultrasound

Ultrasonics is a branch of acoustics that studies sound pressure waves in a range of frequencies higher than the upper limit of human hearing, which is 20 kHz [28].

Ultrasound (US) has the same physical properties as other waves, so it can be reflected, absorbed and focused [28]. The concept of US is to transmit the pressure waves through any media with frequencies above 20 kHz. Ultrasound has been widely used in medicine mainly as an imaging technique [29], but its use in the last three decades has dramatically increased due to new discoveries and possible applications.

One of the recent applications of US is its use in cancer treatment, because it has a positive (synergistic) effect on the treatment efficiency, while contributing to a decrease in the side effects of conventional chemotherapy [30]. US can be categorized as high-intensity and low-intensity. Low-intensity US is used for medical imaging and, to a lesser extent, for treatment purposes, while high intensity US is researched as a treatment constituent to many types of cancers [31]. Ultrasound has been widely used in medicine in general; however, high-frequency US is gaining more attention in cancer treatment due to the fact that it is easily focused on the tumor in comparison with low-frequency US [12, 32]. This aids in efficiently controlling the release of chemotherapeutic agents from drug carriers, as will be explained shortly. Furthermore, an increase in the US frequency allows the acquisition of clearer images of the tumor, which helps in the drug release process without the need for extra instruments [9]. Additionally, it enhances the drug uptake in cells and tissues and facilitates the dissolution of clots for the treatment of blood strokes [29]. Additionally, US is non-invasive and thus the disadvantages of surgery can be avoided [9].

In *in vitro* drug release and cancer treatment research studies, the use of fluorescence techniques can be done in two ways: (i) the *offline* method where the sonication of the sample is done externally and then the fluorescence level is measured afterwards; and (ii) the *online* method which involves the use of a sonication chamber fitted with a fluorescence measurement device [33]. In the sonication chamber, an ultrasonic exposure of the sample happens while simultaneously and continuously monitoring the fluorescence level using a fluorescence detector. The release studies can be done when a fluorescence molecule is encapsulated inside the nanocarrier at self-quenching concentrations. Doxorubicin, mentioned previously, is a fluorescent

molecule, absorbing light at 488 nm and emitting fluorescent light between 530 and 630 nm [27, 34].

Ultrasound is applied using a transducer with a known frequency, measured by a hydrophone placed in the chamber. The fiber optics use lasers to detect the fluorescent changes during the application of US and the data is collected and analyzed [27, 35]. A simple US chamber is shown in Figure (2-2):

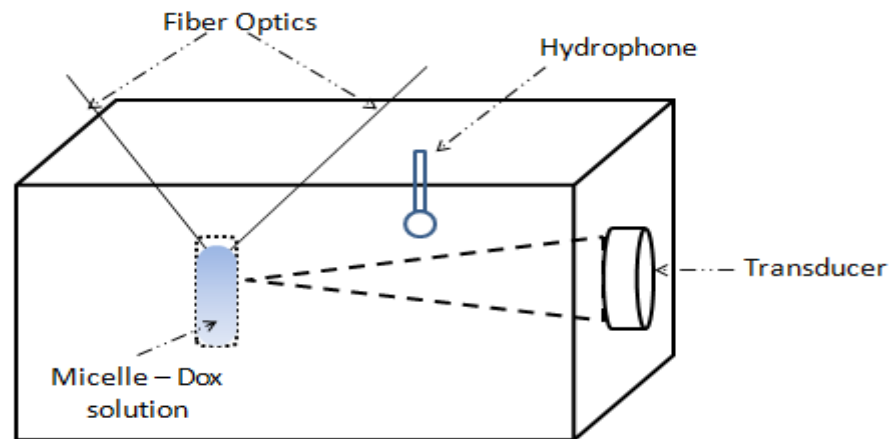


Figure 2-2: Ultrasonic exposure chamber [25, 34].

When US is used in DDS it causes thermal and non-thermal effects on the body organs and tissues. The thermal effect is usually referred to as hyperthermia which results because energy is absorbed by tissues and body fluids causing a rise in temperature that may lead to the death of healthy cells. However, by choosing the proper parameters for the US, including its frequency and intensity, hyperthermia can be controlled and used as an effective modality in cancer treatment [14, 19, 36]. Furthermore, in some DDS, the drug carriers are synthesized in a way such that they are sensitive to temperature, e.g. temperature sensitive liposome (TSL). By using US to raise the temperature of the tumor site, drug carriers found in the vicinity of the tumor will be induced to release their content, hence mediating the process of drug delivery [37-39].

The non-thermal effect is mostly the cavitation of air bubbles, caused by their oscillation [19, 36]. Several studies suggest that the release of molecules from micelles exposed to US is due to cavitation. There are two main types of cavitation: *stable cavitation* which is the continuous oscillation of the bubble without collapsing, and *collapse (transient) cavitation*, where the bubbles collapse aggressively, generating

shock waves and causing a large temperature and pressure rise. The stable cavitation happens at low US intensities while the collapse cavitation happens at high intensities [33, 40]. The effect of cavitation on micelles is shown in Figure (2-3).

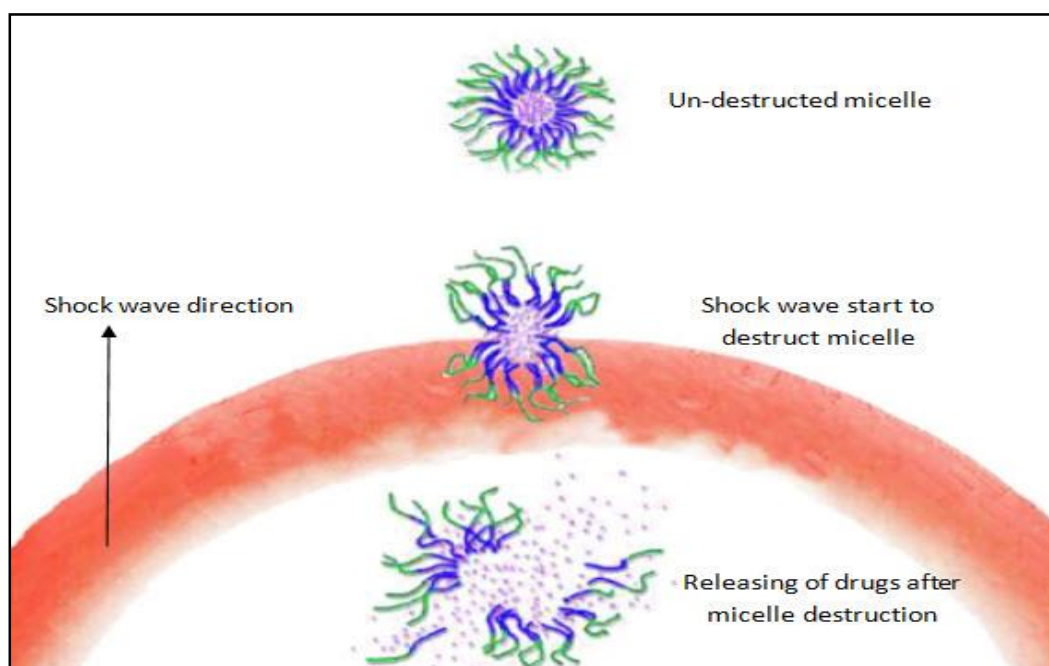


Figure 2-3: The effect of cavitation events on the release of drugs from polymeric micelles [12].

When a microbubble collapses, a shock wave is generated along with an extreme increase in the temperature for a very short period. This shock wave propagates in the surrounding medium, where micelles may be found. If micelles happen to be in the near field of the wave, they get destroyed as the polymeric chains forming the micellar structure lose their association due to the high energy generated by the wave. This will lead to the release of the encapsulated drug [33].

Based on literature data, it was noticed that the release process from micelles triggered by US can be divided into three phases. The first phase is the rapid initial phase where most of the Dox is released. The second phase entails the start of the slow release, while in the third and final phase partial recovery is initiated, where some of the Dox molecules slowly start to re-encapsulate. The graph in Figure (2-4) shows these three phases [10].

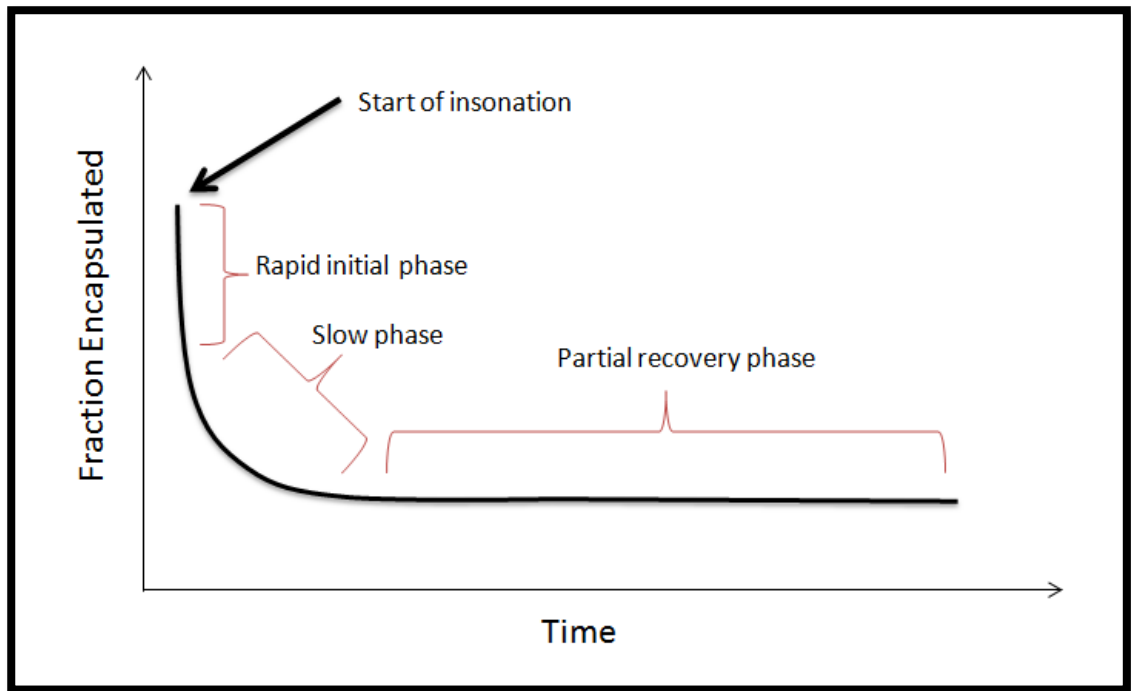


Figure 2-4: Phases of drug release from micelles in the presence of US [40].

2.3. Targeting

There are three main types of drug targeting: *passive*, *triggered* and *active*. The main objective of these mechanisms is to get the best treatment results when using nanoparticles in chemotherapy by increasing their effectiveness [15, 32].

Passive targeting depends on the increased permeability of the vasculature observed in some pathological conditions, such as tumors. This permeability varies depending on the condition and the type of organ affected. The presence of a leaky vasculature at the site of the tumor facilitates the extravasation of carriers and hence the chemotherapeutic agent, which will enhance the release of drugs to the target and increase its cellular uptake. This phenomenon is known as enhanced permeation and retention (EPR) [41].

Besides passive targeting, the drug release from micelles on the targeted tumor can be enhanced by triggers or stimuli, including electric field, pH, temperature and US, a process known as *triggered targeting*. The type of trigger to be used depends on the type of micelles, the drug, and the surrounding environment of the tumor [15, 42]. Ultrasound, which has been previously discussed, is considered one of the best trigger mechanisms in triggered drug delivery [17].

In micellar DDS there are many factors that can be studied and modified to achieve the best treatment results including micellar composition, tumor location and the drug itself. One of the most important micellar components which can be modified to improve and enhance the outcome of the treatment is the surface of the nanocarrier. The type of chemical modification depends on the type of receptor present on the surface of the tumor cells [15, 43]. This type of surface modification is called *active targeting* and can be generally defined as the use of targeting moieties or ligands for enhanced delivery of nanoparticles to the target site.

Choosing the best targeting moiety is important because it affects properties including circulation time, cellular uptake, affinity, and extravasation [44]. Several types of moieties have been investigated including peptides, antibodies, hormones, aptamers and low molecular weight ligands such as folate [45, 46]. These targeting moieties are discussed below, in more detail.

2.3-1 Peptide-based moieties

Peptides are chains of amino acids linked by peptide bonds, and are considered excellent targeting moieties. Due to their small size, ease of manufacture, and low cost, they are one of the most common moieties used in DDS. They can be easily identified using binding regions of a protein or known hormones such as bombesin, by phage display techniques [47], or with the one-bead one compound (OBOC) method [48, 49].

It has been shown that peptides can be used in the targeting and treatment of lung, prostate and ovarian cancer. Also, they can be used to optimize the treatment of T- and B-cell lymphoma. More recently, peptides have been used as targeting moieties in multifunctional nanoparticles used in cancer therapy and imaging [48, 50].

2.3-2 Antibody-based moieties

The use of antibody-based targeting molecules was pursued due to their variety and their specificity for cancer receptors. Monoclonal antibodies (mAb) were the first type of targeting molecules to be used in drug delivery research. With the development of cancer treatment strategies, many new types of targeting antibody moieties were discovered and studied worldwide [51, 52].

There are two types of antibodies depending on how they are obtained. Some are human and some are non-human (developed in labs). In the case of using non-

human antibodies as moieties, they may induce an immunogenic response in the human host. In order to decrease this immunogenicity new methods focused on obtaining chimeric, fragmented and humanized antibodies were developed [48, 52]. Some of these antibodies showed high efficiency when used in targeting: Rituximab has been used in B-cell lymphoma treatment [53], Trastuzumab has been used with HER2 antibody for breast cancer treatment [54], Bevacizumab was designed to inhibit angiogenesis and for the treatment of ovarian cancer [55, 56], and Cetuximab is utilized in advanced colorectal cancer treatment [57].

2.3-3 Aptamer-based moieties

Aptamers are ligands of small nucleic acids that can bind to their target with high specificity, due to their ability to fold into unique three-dimensional conformations [48]. Their use as targeting moieties began in 1990, as an alternative to antibodies to avoid their associated side effects. They have been utilized in targeting different proteins including transcription factors and cell surface receptors [48, 58].

Aptamers have many advantages over other moieties: they show no immunogenicity, they are more stable than antibodies, and there is a consistency between different batches because they are chemically synthesized [58].

Aptamers can be easily produced *in vitro* using the SELEX (Systematic Evolution of Ligands by Exponential Enrichment) procedure, which does not employ any animal cells. Before using the SELEX procedure, it is important to identify and distinguish between cancer cells in order to select which aptamers to use [58]. RNA aptamers can be easily derived using the SELEX process. As an example, the aptamer-siRNA has been developed to bind to the Prostate Specific Membrane Antigen (PSMA), a cell surface receptor that can be found on prostate cancer cells [58, 59].

2.3-4 Small molecule-based moieties

Small molecules are widely used to chemically modify drug carriers used in drug delivery in cancer treatment, due to their diverse structures and ease of production using inexpensive means. The most important small molecule used in targeting is folic acid (folate), but carbohydrates (e.g., galactose, mannose, etc.) have also been studied extensively [48].

Folate is the water-soluble vitamin B9, essential for several processes including cell growth and division. Its use in drug delivery and targeting is related to its binding

to the folate receptor (FR), which is widely expressed on the surface of some cancer cells, including ovarian, brain, kidney, breast, lung and others [48, 60]. Folate easily recognizes the FR and, due to their high affinity, folate molecules bind to FRs. The inclusion of folate in a DDS (anti-cancer drugs and nanoparticles), makes it very useful for both imaging and therapeutic purposes [45, 61].

2.4. *In vitro* and *in vivo* work

There are several scientific reports describing the use of US to release drugs from micelles *in vitro* and *in vivo*, as recently reviewed by Ahmed *et al.* [19].

In vitro studies using cell cultures are very useful in order to design *in vivo* experiments using animal models. Several studies have been reported to study the release of drugs from micelles upon the application of US. Different factors and environments were studied to improve this DDS. Some of these factors are related to US, including power density, frequency and duration of sonication, while others are related to the polymer properties and the drugs used. All of these studies aim to make these systems suitable and safe for human use [13, 19, 34]. Currently there are several ongoing clinical trials using polymeric micellar systems for drug delivery in cancer patients [62], and micelle-encapsulated Paclitaxel (a product called Genexol®) has been approved by the FDA for the treatment of breast cancer [42]. However, the combination of micelle-encapsulated drugs and US has not been used in clinical trials.

2.4.1. *In vitro* work

In vitro release studies suggest three different mechanisms by which US enhances the drug release from micelles [19]. The first one considers that the drug release induced by US occurs outside the cells, and is followed by the drug entering into the cells by a normal diffusion process. The second suggested mechanism considers that the endocytosis of micelle-encapsulated drugs is enhanced by US. The third mechanism states that the cell membrane is transiently perturbed by the application of US, allowing for the transport of released or encapsulated drugs into the cells. The *in vitro* studies provided evidence that the use of US both releases the drug from the micelles and creates transient pores in the cell membranes through which the drug can enter into the cell cytosol. The endocytotic mechanism, however, also seems to play a role in the process.

The release of drugs from polymeric micelles is more efficient when US is applied at low frequencies, as established by the work of Hussein *et al.* [17]. They used Pluronic® P015 micelles containing either Dox or its paramagnetic analogue Ruboxyl (Rb), and exposed them to different frequencies of US, between 20 kHz and 90 kHz, observing that the drug release was higher at the lower frequency. They also studied the effect of varying the sonication intensity and observed that an increase in power density at the same frequency caused an increase in drug release. It was also observed that at lower micelle concentrations of 0.1%, the release was higher compared to the higher micellar concentration. Furthermore, it was observed that the re-encapsulation of drugs between pulses resulted in a decrease of the harmful effects associated with Dox on non-cancerous tissues.

The same group conducted a study to investigate the mechanism and kinetics of Dox release from P105 micelles [10]. Four simultaneous mechanisms were proposed using the assumption of four different micelle sizes. The proposed mechanisms were divided into two parts, the first included destroying and re-assembly of the micelle, while the second included the releasing and re-encapsulation of Dox. It was assumed that the micelles' destruction was due to the cavitation effect which makes cavitation nuclei collapse. Finally, a kinetic model was built for these proposed mechanisms and this model was consistent with the assumption that the collapse cavitation plays a strong role in release phenomena observed experimentally.

Hussein *et al.* [22, 30] also compared the Dox release from regular, unstabilized Pluronic® P105 micelles and stabilized NanoDeliv™ ones. Using 70-kHz US they observed a higher release from unstabilized micelles [22]. Additionally, the study of the release kinetics showed that the Dox release rates from unstabilized micelles were significantly higher than those from stabilized ones [30].

The first study on the effects of the use of micelle-encapsulated drugs in conjunction with US, on cancer cell cultures was described by Munshi *et al.* [63]. They reported a synergistic effect when using 80-kHz US and Dox encapsulated in Pluronic® P105, with the drug IC₅₀ decreasing in the presence of US.

Hussein *et al.* [11] performed an *in vitro* study using the HL-60 cancer cell line to test the effect of the drug Dox on the cell DNA. Dox is known to be one of the most effective drugs against cancer. However, traditional methods of delivery had a

shortcoming, as the drug was injected and allowed to freely circulate in the blood stream, thus affecting both healthy and cancerous cells. This gave rise to the need for more directed DDS, hence the use of targeted micelles. Dox was delivered in two ways: the first was by directly adding it in its free state, and the second was through encapsulating it inside Pluronic® P-105 micelles. The results were collected with and without insonation. It was observed that when free Dox was used in the presence of 70-kHz US, the damage to cells was higher in comparison with the use of free Dox. However, it was observed that when Dox was delivered encapsulated in micelles under the influence of US, the DNA damage was significantly higher and 96% of the cancer cells were dead after 2 hours of exposure. Importantly, this study also established that the mode of cell death was apoptosis and not necrosis.

In another investigation, the relation between drug release and high frequency US (1 MHz) was tested [64]. The tests were conducted on different types of cancer cell lines including leukemia HL-60 cells, drug-sensitive ovarian carcinoma and breast cancer MCF-7 cells. It was hypothesized that when using US, cavitation events occurred that could be monitored by quantizing the associated free radicals using a process called radical trapping. It was observed that there was formation of radicals with changing frequencies and power densities. The cavitation threshold intensity increased as the US frequency increased as observed when monitoring free radical formation at different frequencies. It was noticed that, at higher frequencies, although transient cavitation almost ceased to exist, drug release was still observed, indicating that drug release from micelles was not tied to transient cavitation. It was also found that the rate of cellular uptake of Dox was higher even at short time exposures to high frequency US.

Another factor investigated was the effect of the pulsing time dependency of the drug uptake. The work of Marin *et al.* [65] showed that the US-triggered release from micelles did not occur at time pulses shorter than 0.5 s, resulting in a low concentration of drugs in the medium of incubation. For time pulses longer than 0.5 s, the release was noticed and the concentration of the free drug increased [65].

Later, the same group [30] conducted more experiments on the release of anti-neoplastic medications from micelles triggered by US. The study was done using a fluorescence detection exposure chamber, similar to the one described earlier, to investigate the release and re-encapsulation of Dox from micelles. They found that at a

power density of 58 mW/cm² and 20 kHz, no noticeable release of Dox occurred after exposure to US for less than 0.1 s. The group also developed a mathematical model for the release and re-encapsulation that was zero-order in release and first-order in re-encapsulation.

The mechanism of US-enhanced cellular uptake has been extensively studied, and different studies have shown different results. Tachibana *et al.* conducted several experiments to study the effect of US on the permeability of cell membranes [66, 67]. In one of their early studies [68] HL-60 cancer cells were sonicated at an intensity of 0.4 W/cm² with a continuous frequency of 255 kHz in the presence of merocyanine 540 (MC 540) as a drug/tracer. The sonication was done for a period of 30s, and electron microscopy was used to observe the effect of US on the surface of the cells. The authors observed the formation of pores in the cell membranes that led to their death. They latter concluded that the cell death was caused by both the drug and the US treatment [67]. To confirm their theory, the same group conducted another experiment using the cytosine arabinoside drug with HL-60 cells sonicated at 48kHz US with an intensity of 0.3 W/cm² [66]. The results of this study showed that the cell death increased upon sonication, when compared to a sonicated control sample, not exposed to the drug. This suggested that cell membrane permeability increased when subjected to US, allowing for the diffusion of the drug through the transient membrane pores into their cytosol and leading to their death [66, 67].

The effect of US on cell membrane permeability was later studied by Schlicher *et al.* [69, 70]. This group used DU145 prostate cancer cells that were sonicated at 0.36, 0.54, and 0.71 atm for the duration of 0.1s at a frequency of 24 kHz [69]. This group hypothesized that the formation of pores in the cell membrane upon sonication was due to cavitation events induced by US [71]. They also suggested that the size of the pores formed increased with the increase of cavitation events, which was proportional to the sonication intensity. Later, a study done by Zhou *et al.* [72] used the voltage clamp technique to measure the size of the pores formed by the application of 1.075 MHz US (0.2 s, 0.3 MPa) in *Xenopus laevis* oocytes. The results were in agreement with the previously suggested relation between frequency and sonoporation.

However, several other studies suggested a different mechanism for increased cell death due to the treatment of chemotherapy along with sonication. These studies observed an increased endocytotic activity when US was applied, without any

significant cell membrane deformations, thus excluding sonoporation as the main mechanism [73, 74].

Muniruzzaman *et al.* [75] obtained evidence that suggested the uptake of micelles by cells occurs via fluid-phase endocytosis. The aim of their study was to test the effect of the aggregation state on the intracellular uptake of Pluronic® P105 micelles by HL-60 promyelocytic cancer cells. The results showed that, below the CMC, the cell uptake increased with the increasing concentration of micelles in the incubation medium, while above the CMC, the intracellular uptake was less efficient. This suggested that below the CMC the unimers enter the cell via diffusion through the cell membrane, while the micelles enter the cell via endocytosis. Similarly, the studies by Rapoport *et al.* [76] and Sheikov *et al.* [77] provided evidence for endocytotic events.

Since different studies provide evidence for different mechanisms by which US increases drug uptake, the topic is still undergoing research. It is worth mentioning that, although most of the studies involving micelles and US as a DDS are usually done using Pluronic®, many other types of micelles used in drug delivery research have been described in the literature. For example, Howard and co-workers [78], synthesized micelles of methyl-capped poly(ethylene oxide)-co-poly-(L-lactide)-tocopherol with encapsulated Paclitaxel and sonicated the samples at 1 MHz and 1.7 W/cm² intensity US to study the effectiveness of this DDS in human breast adenocarcinoma (MCF7) cells. The results proved the viability of US usage as a triggering mechanism by which the release from micelles could be controlled. The results also showed the importance of using micelles to encapsulate drugs, which aids in reducing the side effects observed when the drug is introduced in its free form. Zhang and co-workers synthesized a different type of polymeric micelles using a block copolymer containing poly-lactic acid-b-polyethylene glycol (PLA-b-PEG), loaded with the Nile Red stain and used HIFU to trigger the release from the micelles. They measured the release by measuring the Nile Red stain level before and after sonication and the results showed that HIFU can trigger the irreversible release of Nile Red, by the principle of transient cavitation. The release could be controlled by tuning the properties of US such as intensity, time and the location where it is focused [79].

Other research, such as that described by Chen *et al.* [80], use Pluronic® mixed micelles to encapsulate low solubility compounds such as docetaxel. The system was

used in a human lung adenocarcinoma cell line resistant to the anti-cancer drug Taxol, and its effects were enhanced when compared with the use of free docetaxel.

Ugarenko *et al.* [81] also studied the release of Dox and formaldehyde-releasing prodrugs from stabilized mixed Pluronic® micelles using 20-kHz US at high power densities (100 W/cm^2). They observed that when micelles were formed, 60% of Dox was encapsulated with a retention half-life of approximately 12 hours. It was observed that at such US power densities, 7-10% of the encapsulated Dox was released. On the other hand, the formaldehyde-releasing prodrugs were not encapsulated inside the micelles, but it was observed that these could be used separately to enhance the formation of Dox-DNA adducts in tumor tissues. The same group tested the effect of this micellar system in Dox uptake by breast cancer cells MDA-MB-231, and observed that, in the absence of US, the uptake was reduced when compared to the application of the free Dox. Upon application of 20-kHz, 100 W/cm^2 US, the drug was released from the micelles and the cellular uptake was increased.

2.4.2. *In vivo* work

In vivo studies with animal models are extremely important as preclinical experiments, and the most common models used to conduct *in vivo* experiments are mice and rats inoculated with a known type of cancer cell lines that will generate a tumor. The lab animals are then treated with Dox or other chemotherapeutic drugs, encapsulated in micelles or in free form, to compare the efficiency of the different DDSs, with and without exposure to US. The results of the inhibition of tumor growth are compared and if the success rate is high enough and the side effects are acceptable, clinical trials on human subjects may be the next step.

One of the first *in vivo* studies with micelles and US used a colon carcinoma (DHD/K12/TRb cells) rat model to investigate the effect of Dox concentration, US frequency and power density, among other variables [82]. The tumors were induced into the rats' legs by injection with the tumor cells, and treated with Dox at different concentrations. The Dox was encapsulated into stabilized Pluronic® micelles and was administered weekly for a period of 6 weeks. One of the legs was exposed to 70-kHz US, while the tumor on the other leg was not US-treated; hence it was used as a negative control. It was observed that the higher concentrations of encapsulated Dox were lethal to the animals: 4 and 5.33 mg/kg were lethal within 6 weeks, while 8 mg/kg killed the

animals within 2 weeks. The treatment with micelles encapsulating Dox concentrations of 1.33 and 2.67 mg/kg combined with the use of US were found to be the most effective in fighting the tumor cells.

The same rat model was used by Staples *et al.* [83] to investigate the effects of Dox encapsulated in stabilized Pluronic® micelles (NanoDeliv™) triggered with low (20 kHz) and medium (476 kHz) frequency US [83]. The study compared the results of treating the rats using micelles, with and without US. It was expected to get better results when using the combination of micelles with sonication, since *in vitro* experiments proved the sensitivity of Pluronic® micelles to US. The results of the study showed that tumor growth in this later case decreased when compared with tumors treated with micelles only (no US). The study further explored the growth or remission behavior of tumors and it was found to fit an exponential model for both the control and insonated tumors at 20 kHz and 476 kHz [83].

The same research group used a tumor-bearing rat model to investigate the effect of using US on the treatment. They found that when the drugs were delivered using US, the results were better at both increasing the death of cancer cells and decreasing the damage on healthy cells. The variation of US frequency did not show any effect on tumor growth; it was observed that frequencies of 20 kHz and 476 kHz produced very similar results [14].

Another study by Rapoport and co-workers [84] investigated the advantage of using Dox encapsulated in Pluronic® micelles and -MHz high frequency US to treat immuno-compromised athymic nu/nu mice, injected with ovarian carcinoma tumors. The fluorescence level upon sonication was measured in the heart, kidneys, liver and spleen and the results were compared to the case when the tumors were not sonicated. The objective of the study was to examine localized drug release controlled by US compared to the non-localized release due to the natural degradation of micelles. The fluorescence level was found to be dramatically lower in the heart when US was used, which suggested that the cardiac toxicity of Dox could be greatly decreased when using micelles. The results also showed a sharp decrease in drug uptake by kidney cells, while the uptake by liver and spleen cells was greatly enhanced. It was concluded that focused US decreases the drug spread and uptake by healthy tissues, while increasing the drug uptake locally.

The synergism between the use of encapsulated drugs and US was also emphasized in a recent study by Hasanzadeh *et al.* [85], using a mouse model. In this study, adult female mice were inoculated with spontaneous breast adenocarcinoma tumors and were divided into three groups: (i) the tumor was treated with a 1.3 mg/kg dose of free Dox; (ii) the tumor was treated with the same concentration of Dox but encapsulated in Pluronic® P105 micelles; (iii) the tumor was treated using the same concentrations of encapsulated Dox and, in addition, sonicated at 28-kHz and 3-MHz US. It was observed that the drug accumulation in tumor cells was enhanced in the third group compared to first and second groups by 8.69- and 2.60-folds, respectively. Another observation was that the uptake by the healthy cells and organs was lower in the third group: 3.35- and 2.48-fold when compared to the first and second groups, respectively. The results of this study clearly support the improvement that US along with micelles can provide when used as a DDS.

Chapter 3 : Theoretical Analysis

As mentioned above, the model used in this work was previously published in two papers [9, 10]. The first paper [10] proposes simultaneous mechanisms for the process of drug release, and it assumes the mechanism to be first order. The mathematical summary of this physical mechanism is given below.

- The micelles used are Pluronic® P105 with a diameter ranging between 10 and 20 nm. The micelles are divided into five groups based on the diameter of the micelles. Each group contains 20% of the polymer, then the fraction of the total number of micelles ($M_{j,o}$) can be calculated using equation (1):

$$M_{j,o} = \frac{\left(\text{volume of polymer} / \text{volume of one micelle} \right)_j}{\sum_{i=1}^n \left(\text{volume of polymer} / \text{volume of one micelle} \right)_i} \quad (1)$$

- The number of micelles changes with time due to two competing mechanisms: the first is the destruction of the micelles, and the second is their reassembly. The change in the number of micelles with time is given by equation (2):

$$\frac{dM_j}{dt} = \left(\frac{dM_j}{dt} \right)_{\text{destruction}} + \left(\frac{dM_j}{dt} \right)_{\text{assembly}} \quad (2)$$

- a) The rate of micelle destruction is given as follows:

$$\left(\frac{dM_j}{dt} \right)_{\text{destruction}} = -k_{a,j} M_j N \quad (3)$$

where, $k_{a,j}$ is the rate constant which depends on the size of the micelles, with the following proportional relationship:

$$k_{a,j} = \alpha \bar{D}_j \quad (4)$$

where α is a non- zero constant during insonation

N is the number of cavitating nuclei, and its value is assumed to decrease slowly with time because of bubble collapsing which happens at all power densities used to collect the release data. The rate of this decrease is given by:

$$\frac{dN}{dt} = -k_N N \quad (5)$$

If equation 5 is integrated, the resulting solution is:

$$N = \exp(-k_N t) \quad (6)$$

b) The rate of micelle reassembly is given as follows:

$$\left(\frac{dM_j}{dt}\right)_{assembly} = k_{a,j} V_{FP} \quad (7)$$

$k_{a,j}$ is a rate constant that depends on the size of the formed micelles. The formation here depends on the polymer volume, so the constant can be related to the inverse of the diameter cubed:

$$k_{a,j} = \frac{\beta}{(D_j^3)} \quad (8)$$

V_{FP} is the normalized volume concentration. It can be obtained by dividing the volume of free polymers in the solution, v_{FP} by the volume of the solution, v_{sol} ; then normalizing this value by the concentration if the polymer chains are freely available in the solution $v_{tot,o}/v_{sol}$:

$$V_{FP} = \frac{v_{FP}/v_{sol}}{v_{tot,o}/v_{sol}} = \frac{v_{FP}}{v_{sol}} \quad (9)$$

The volume of free polymers v_{FP} is equal to the initial total volume minus the volume at any time, then:

$$V_{FP} = 1 - \frac{v_{tot}}{v_{tot,o}} \quad (10)$$

Now, we need to relate the total volume to the volumes of all micellar groups:

$$V_{FP} = 1 - \frac{\sum_{j=1}^n M_j (\pi/6) \overline{D_j^3}}{\sum_{j=1}^n M_{j,o} (\pi/6) D_j^3} \quad (11)$$

$M_{j,o}$ is the initial fraction of micelles in group j , which equals $1/n$, hence:

$$V_{FP} = 1 - n \frac{\sum_{j=1}^n M_j D_j^3}{\sum_{j=1}^n D_j^3} \quad (12)$$

- The amount of drug encapsulated changes with time due to two mechanisms: the first is the release of the drug after the destruction of micelles, while the second is the re-encapsulation of drugs inside the micelles:

$$\frac{dE_j}{dt} = \left(\frac{dE_j}{dt}\right)_{destruction} + \left(\frac{dE_j}{dt}\right)_{encapsulation} \quad (13)$$

- a) The rate of drug release is related to the destruction of micelles. The drug concentration is assumed to be the average of the drug concentration within its corresponding group:

$$\left(\frac{dE_j}{dt}\right)_{destruction} = \left(\frac{dM_j}{dt}\right)_{destruction} \left(\frac{E_j}{M_j}\right) \quad (14)$$

By using eq. 3,

$$\left(\frac{dE_j}{dt}\right)_{destruction} = -k_{d,j} N E_j \quad (15)$$

- b) After micellar reassembly, the free drug is re-encapsulated. The amount of free drug, F , depends on the capacity of the newly formed micelles. This capacity is the difference between saturation (if the whole capacity is filled) and the actual amount:

$$\left(\frac{dE_j}{dt}\right)_{encapsulation} = k_{e,j} F (E_j^{sat} - E_j) \quad (16)$$

where $k_{e,j}$ is a rate constant which depends upon the ratio of the surface area to the volume, so it is inversely proportional to the micelle mean diameter:

$$k_{e,j} = \frac{\gamma}{(D_j)} \quad (17)$$

The saturation concentration of the drug that can be encapsulated inside the micelles depends on the number of micelles, volume of each micelle and the amount of drugs that can be stored per unit volume, ρ_{Dox}^{sat} :

$$E_j^{sat} = M_j \frac{\pi}{6} \overline{D_j^3} \rho_{Dox}^{sat} \quad (18)$$

ρ_{Dox}^{sat} can be considered as the total amount of drug that can be encapsulated in an initial total volume within the micelles:

$$E_j^{sat} = M_j \frac{\pi}{6} \frac{\overline{D_j^3} E_{tot,o}^{sat}}{v_{tot,o}} \quad (19)$$

The total initial volume $v_{tot,o}$ can be related to the sum of all volumes in all micellar groups:

$$E_j^{sat} = n M_j \frac{\overline{D_j^3}}{\sum_{j=1}^n \overline{D_j^3}} E_{tot,o}^{sat} \quad (20)$$

The total amount of the drug is the sum of the free fraction and the encapsulated fraction, hence the free amount of the drug in the solution, F, is:

$$F = 1 - E \quad (21)$$

The amount of encapsulated drug, E is the sum of all drugs encapsulated in each group:

$$E = \sum_{j=1}^n E_j E \quad (22)$$

In [9], a simplification of the encapsulation model (eq. 16) is described.

It is assumed that the saturation amount of drugs, E_j^{sat} is very large compared with the encapsulated drug amount in group j, E_j . So we assume that E_j is negligible, and equation (16) can be simplified:

$$\left(\frac{dE_j}{dt}\right)_{encapsulation} = k_{e,j} F E_j^{sat} \quad (23)$$

Then by substituting all the terms from the previous equations, we obtain:

$$\left(\frac{dE_j}{dt}\right)_{encapsulation} = \frac{\gamma}{(D_j)} F n M_j \frac{\overline{D_j^3}}{\sum_{j=1}^n \overline{D_j^3}} E_{tot,o}^{sat} \quad (24)$$

The three constants γ , n , $E_{tot,o}^{sat}$ can be incorporated in one single term called the encapsulation parameter, λ :

$$\left(\frac{dE_j}{dt}\right)_{encapsulation} = \lambda F M_j \frac{\overline{D_j^3}}{D_j \sum_{j=1}^n \overline{D_j^3}} \quad (25)$$

The MATLAB program; which what will be discusses later; was developed to calculate all the constants related to release, re-encapsulation and reassembly, namely " $\alpha, k_n, \beta, \lambda$ ". These four kinetic parameters were compared for the acoustic release of Dox from folated versus non-folated micelles. The results obtained were also used to determine if these kinetic rates are a function of power intensity.

Chapter 4 : Data Analysis

4.1. Experimental Procedure

The data used for the modeling process described in this work was collected by Dr. Ghaleb Husseini [86]. The experiments focused on measuring the drug encapsulation percentage for two types of micelles; folated and non-folated micelles. A solution consisting of a buffer added a certain concentration of Pluronic® P105 polymers until the CMC was reached hence ensuring the formation of micelles. Then, the prepared sample was added to a cuvette in preparation for the insonation process

The cuvette was then inserted in the US chamber shown in Figure 2-2 where a 70 kHz US wave was used to induce drug release. The sonication chamber was attached to a fluorescence detector that continuously monitored the fluorescence level of the sample. Before sonication, the fluorescence level was measured for a 10 second period. This period should correspond to a 100% encapsulation level. At the 10 second mark, the US was turned on leading to the release of some of the encapsulated drug. The fluorescence level at this instant should be less than 100% as what is being measured is the percentage of encapsulation. Then, after 10 seconds of insonation, the US was turned off and the fluorescence level was monitored for another 10 seconds leading to a measurement of 30 seconds in total.

The measurements of the fluorescence level were collected using computer software that controled the detector. The samples to read every second could be increased by adjusting the sampling frequency for fast changing measurements. In this experiment, the data assumes two levels, one at 100% and the other at a lower percentage. However, when the data was collected, the sampling frequency was not lowered; hence, the collected data has what appears to be noise. Nonetheless, in reality, the fluctuation in the data is due to the unnecessarily introduced noise caused by the high sampling and high sensitivity of the detector.

4.2. Data Denoising and Preparation

The first step in data analysis was the pre-processing of the raw experimental data, since it contains high levels of noise. Figure (4-1) shows the unprocessed raw data.

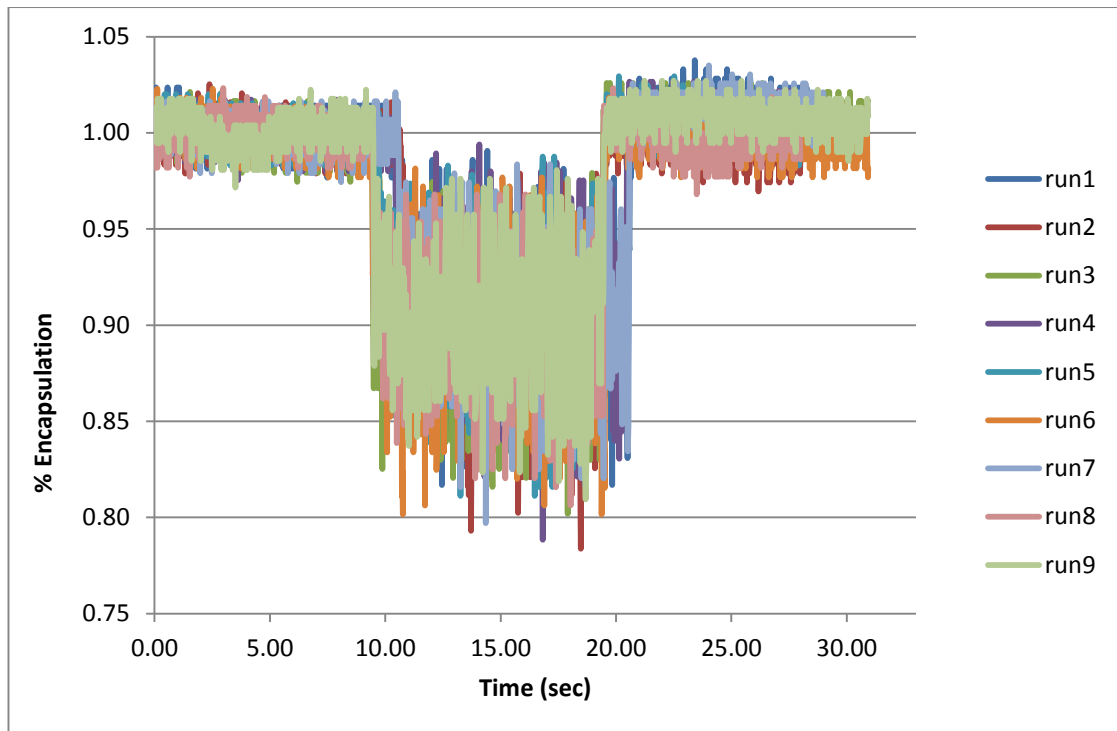


Figure 4-1: Non-processed data showing the temporal release for Folated-P105-2.183.

The data was pre-processed using Microsoft Excel and the MATLAB program as follows:

a) Data overlaying:

Since the US was manually turned *on* and *off*, the experimental results needed to be superimposed to make the *on* and *off* time points coincident. This was done in Excel, by excluding some of the initial data collected before the US was turned *on*. Afterwards a 5-point average was applied in order to reduce the noise. The resulting release/re-encapsulation profiles are shown in Figure 4-2.

b) Data Denoising:

The noise that can be observed in the graph (Fig. 4-2) was reduced using the *wave menu property* in the MATLAB software. This property is based on the wavelet concept which is very robust in denoising data. In MATLAB software, the command *wavmenu* opens a GUI that allows the user to perform dynamic denoising by changing the parameters manually while observing the output continuously. For the purpose of this work, the data was imported into

the GUI run by run and the denoising processes were done for each one. Figure 4-3 shows a sample of this process.

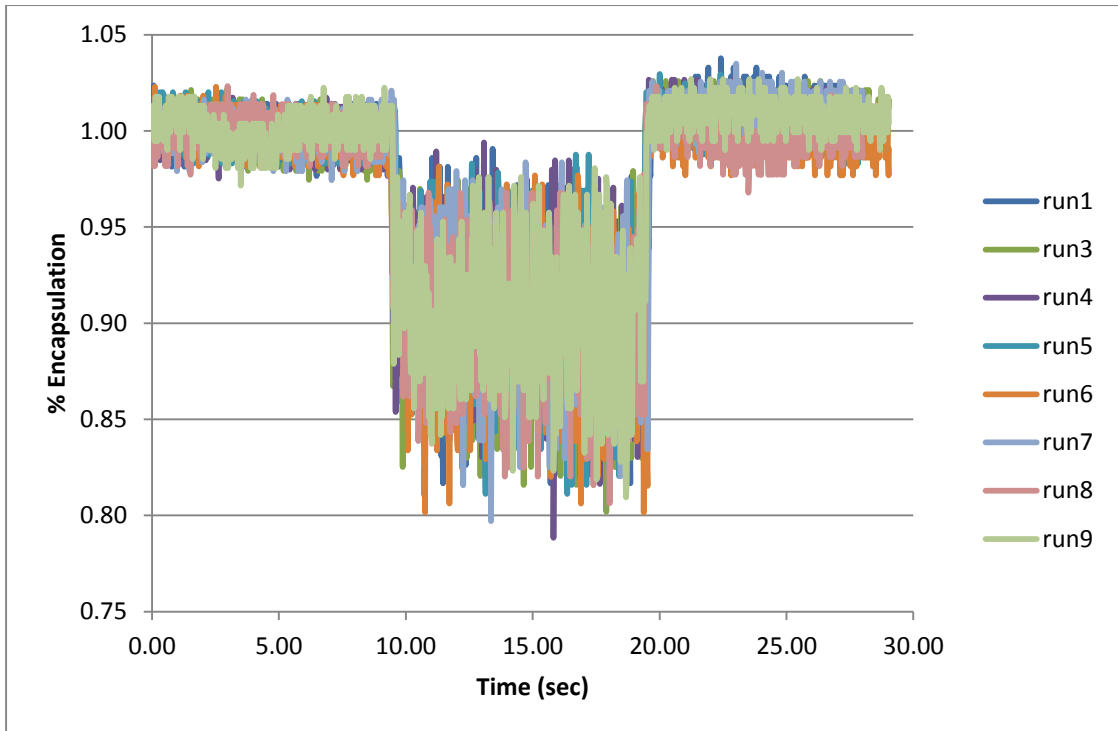


Figure 4-2: Overlaid data showing the temporal % release for Folated-P105-2.183.

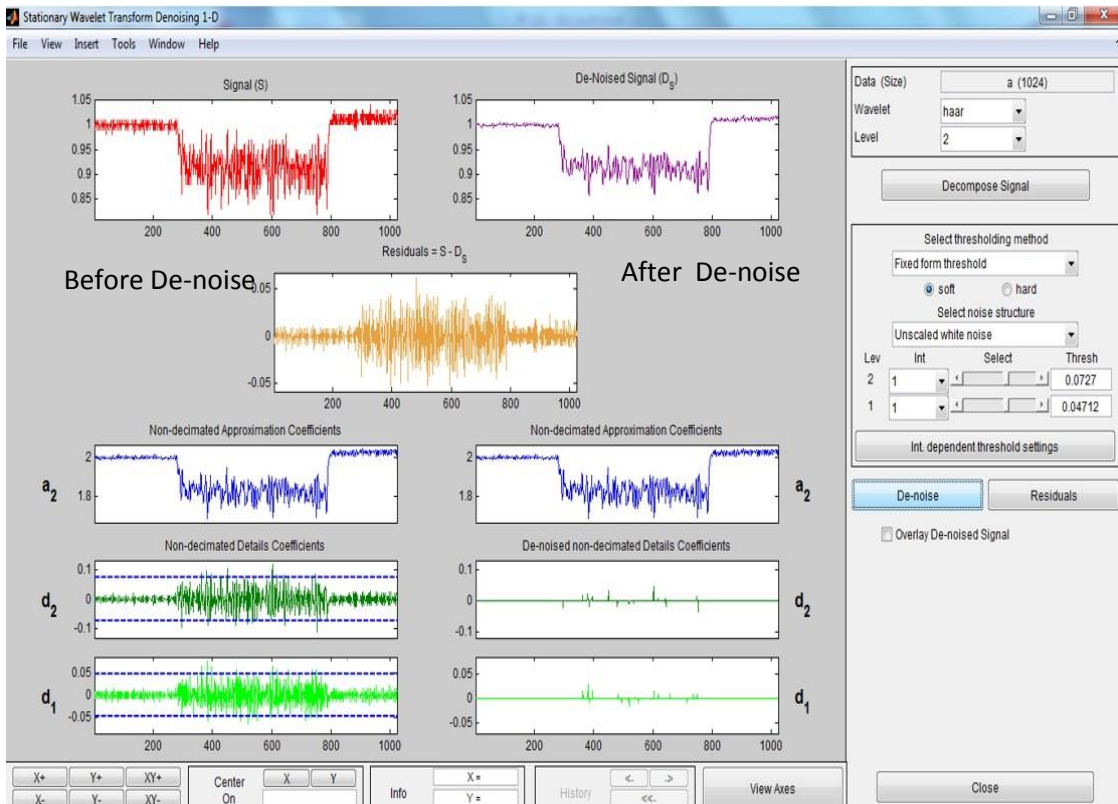


Figure 4-3: Denoising using the MATLAB software.

This procedure was repeated for the total number of runs. The graph was then divided into two parts: the release and the re-encapsulation parts, as shown in Figures (4-4) and (4-5).

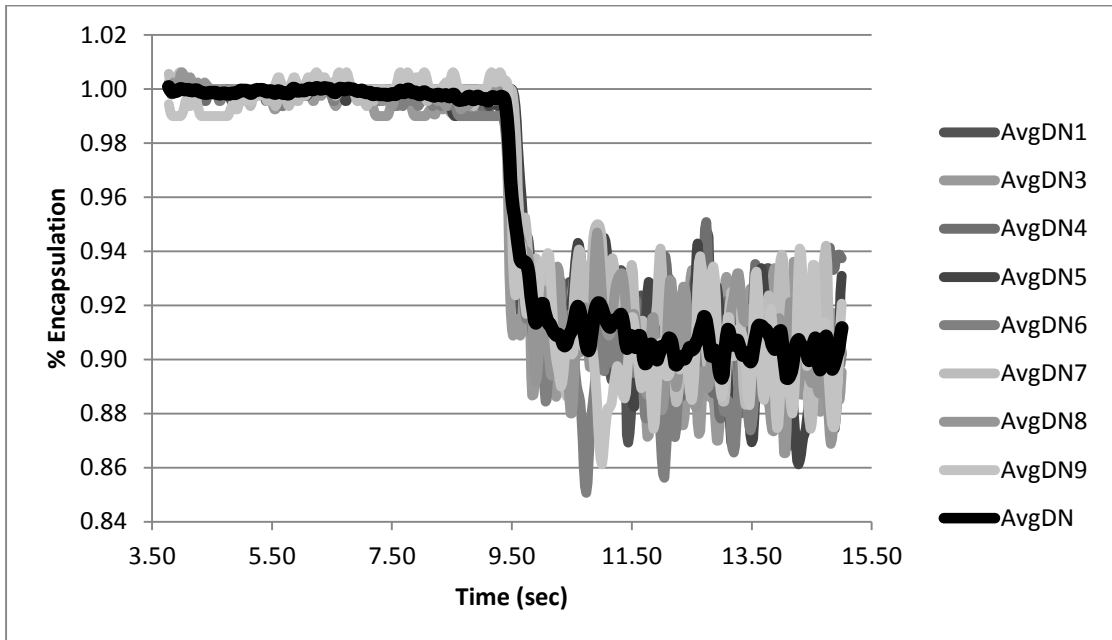


Figure 4-4: Average data showing the temporal release for Folated-P105-2.183 (Release part).

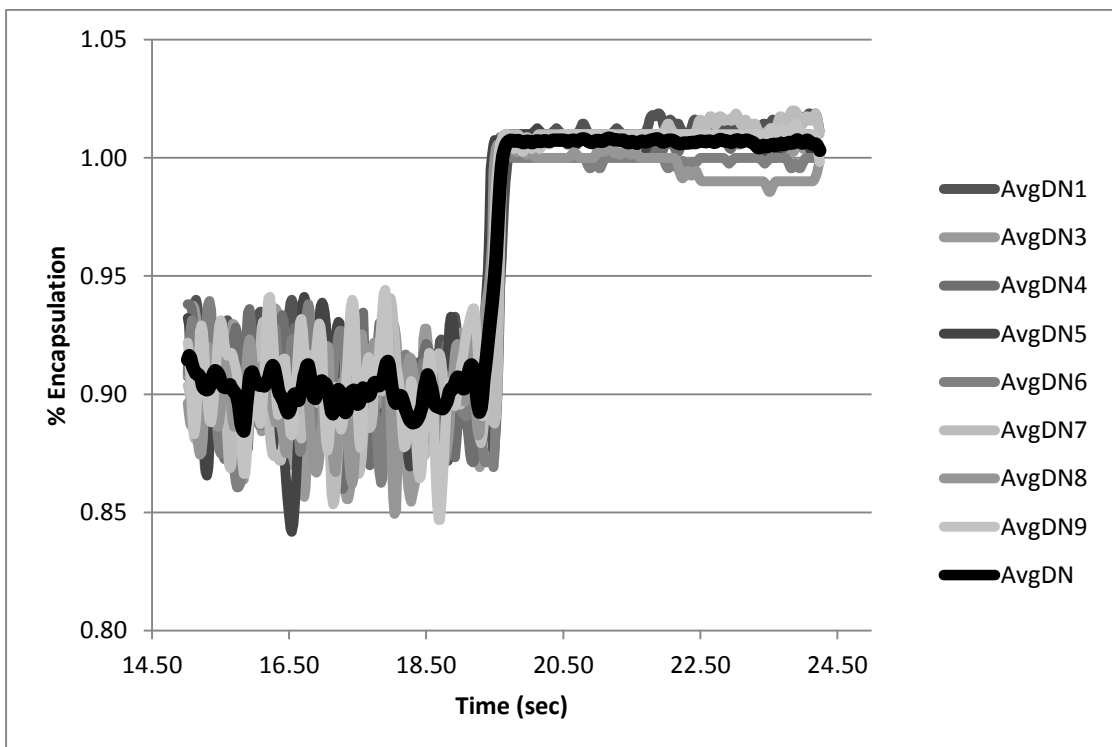


Figure 4-5: Average data showing the temporal release for Folated-P105-2.183 (Re-encapsulation part).

4.3.Data Modeling Using the MATLAB Designed Program

The model described previously is the basis of this study, and data modeling was hence used to calculate the kinetic parameters involved in the acoustically activated release of Dox from Pluronic micelles. Simulation was performed using a MATLAB program. The steps for the work were as follows:

- a. The model equations were rearranged as the two following equations:

$$\frac{dM_j}{dt} = [-(\alpha \overline{D_j}) M_j (\exp (-k_N t))] + \left[\left(\frac{\beta}{(\overline{D_j}^3)} \right) \left(1 - n \frac{\sum_{j=1}^n M_j D_j^3}{\sum_{j=1}^n \overline{D_j}^3} \right) \right] \dots \text{(a.1)}$$

$$\frac{dE_j}{dt} = [-(\alpha \overline{D_j}) (\exp (-k_N t)) E_j] + \left[\lambda F M_j \frac{\overline{D_j}^3}{\overline{D_j} \sum_{j=1}^n \overline{D_j}^3} \right] \dots \text{(a.2)}$$

In these two equations, we have four constants (α , β , λ and k_N) that need to be determined. (k_N), which is a constant that is related to the number of cavitating nuclei, is assumed to be zero in the data collected. The (k_N) is calculated from the partial recovery phase. It indicates if there is an upward slope within this phase. In the data used, the recovery phase is almost linear, hence (k_N) is assumed to be negligible. The other three constants have to be determined simultaneously as described above. The modeling process at hand cannot be done analytically, as there are 2 equations with 3 unknowns, so numerical methods were used to represent the kinetics of our system

- b. In order to determine these constants numerically, we designed a MATLAB program based on the *least squares method*. The code contains two files: the *function* file, and the *script* file. In the function file, the main equations used were defined along with their derivatives and the output was returned to the script file to be used in the *least squares equation*. The derivatives of those equations were calculated numerically using the finite difference forward formulas. As an example, the derivatives dM and dE were found as follows:

$$dM_{j(i)} = \frac{M_{j(i+1)} - M_{j(i)}}{dt}$$

$$dE_{j(i)} = \frac{E_{j(i+1)} - E_{j(i)}}{dt}$$

The *least squares method* compares experimental data with the given model, and provides the best fit. Experimental data for our work is the percentage of drug release (E) for two different micelles, folated micelles (folated-P105) and non-targeted micelles (P105). The initial values for the drug amount (E_j) were assumed to be the same for the five proposed groups of micelles: 0.2 for each group. All the needed initial data are presented in Table 4.1.

Table 4-1: Initialization values for the parameters used for the modeling process.

Group (j)	Mean Diameter (nm)	Mean Cubed Diameter (nm ³)	Fraction of total micelles (M)	Fraction of drugs per group (E)
1	11.6	1618	0.372	0.2
2	14	2670	0.226	0.2
3	15	3411	0.177	0.2
4	16.5	4469	0.135	0.2
5	19.6	6765	0.089	0.2

c. In the function file, the two main equations described earlier were adapted for each of the five groups of micelles, i.e. ten equations were entered, five for the (M) and five for (E). Then, for simplicity, the symbols v(1), v(2) and v(3) were used to refer to the constants α , β and λ respectively, and the *least squares method* code was entered with given upper and lower limits within which the result should fall. The code is as shown below :

- Lower and upper limits:

v1b=[0.001;150;50];

vub=[1;1000000;170500];

- Least square code

v=lsqcurvefit(@expected,v,[M1,M2,M3,M4,M5,E1,E2,E3,E4,E5],Ee,v1b,vub)

d. The code was then executed using the data that was collected at the moment the US was turned *on*, until the point after the partial recovery phase such that the entire release profile was taken into the model as shown in Figure (4-6).

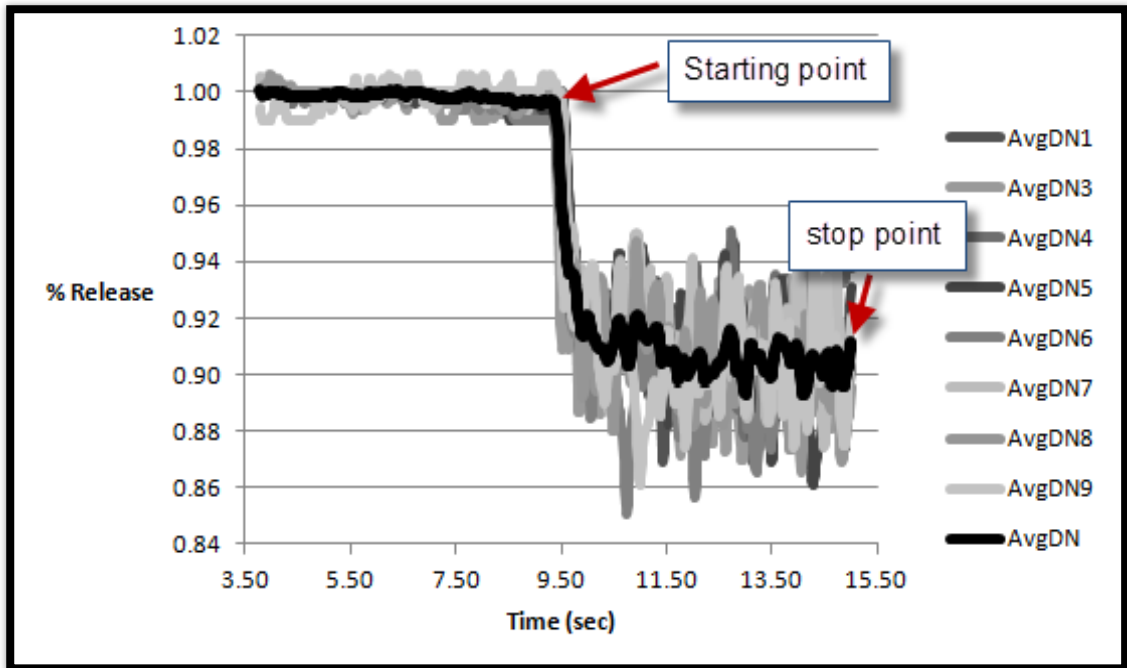


Figure 4-6: Starting and stop point for the modeling.

- e. After exporting the data, the start and end points, as well as the data length for every run were entered and the code was executed. The resultant plot (Figure 4-7) compares the fraction encapsulated vs. time of the experimental data with the kinetic model described above. The code also generates the values for the constants. An example of the result is shown in Figure (4-7).

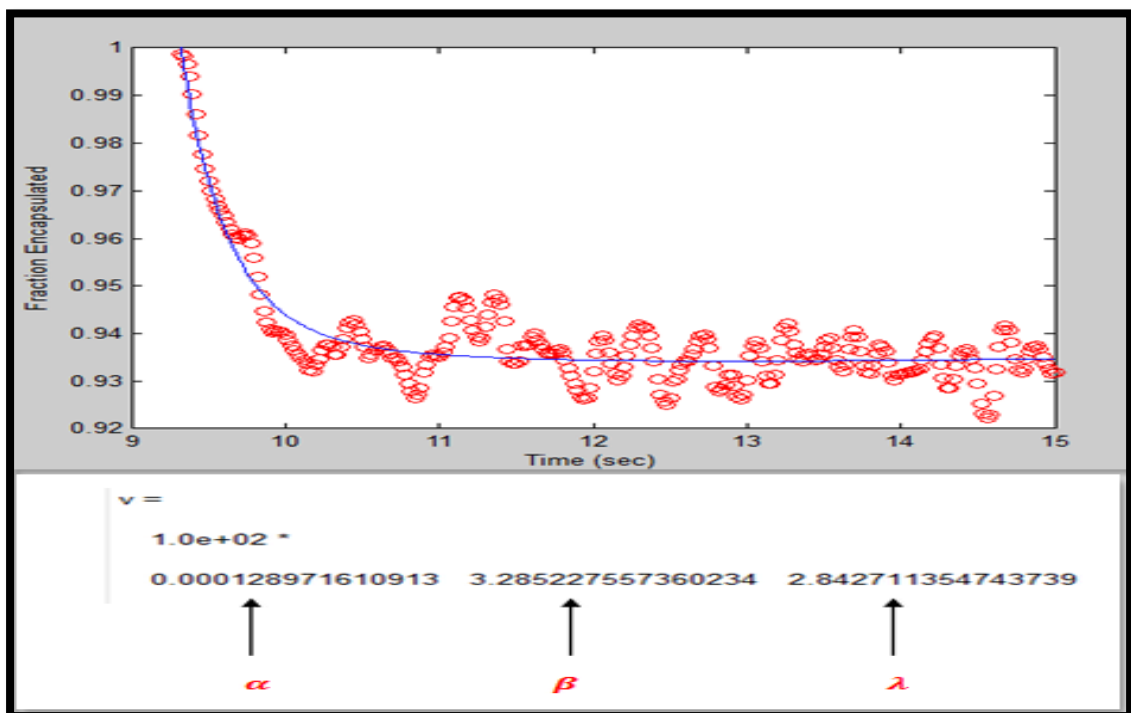


Figure 4-7: The modeling results obtained using MATLAB.

Chapter 5 : Results and Discussion

5.1. Modeling

After preparing the data for the analysis, the code was used to obtain the three constants for every run, followed by the calculation of the average and standard deviations of each constant at every power density. The experiments were done at a 70-kHz US frequency and 37°C. The results obtained for the constants are summarized as follows:

1. Alpha (α):

Table (C-1) in the Appendix shows the results for the first constant (α) for both folated and non-folated micelles. The values were plotted and the graph is shown in Figure (5-1) where results are the average \pm standard deviation of the replicates indicated in Table B.1 in the Appendix.

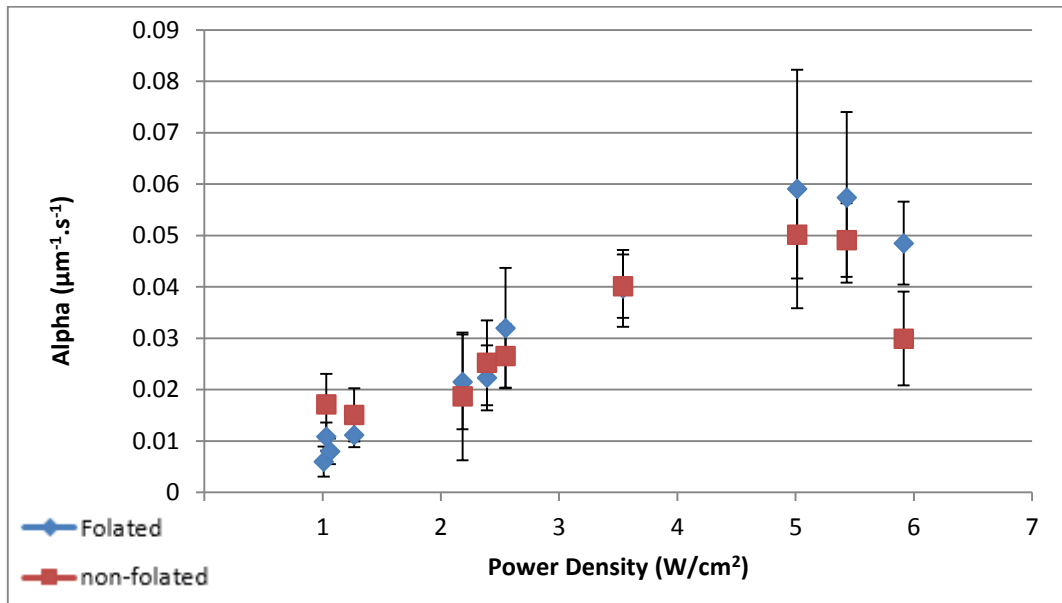


Figure 5-1: The relation between power density and the amount of destruction of micelles which is quantified by Alpha.

α is a destruction parameter which represents how micelles are quickly destroyed upon insonation. Based on the equation of micelles ($\frac{dM_j}{dt}$), as α increases, the amount of micelles (M) decreases, proving the concept that after insonation starts, micelles are rapidly destroyed due to cavitation. It was previously known that α depends on both temperature and the diameter of the micelles, but here we unravel its relation with power density.

Table (C-1) in the Appendix and Figure (5-1) show how α changes with power density for folated and non-folated micelles. It can be clearly seen that α increases with power density except at the last point, which may be due to an experimental error, or a random change in the mechanism that causes the release. For example, the release is assumed to be the result of cavitation, however, at higher power densities, other parameters such as temperature might change and have an effect on the release behavior. All in all, this outlying point opens the door for further research. The differences between the two types of micelles are very small. However, by looking at the graph, it can be seen that the general trend is that α is usually a bit higher for the folated micelles (Folated-P105) than for the non-folated (P105), for the higher power densities. This might indicate a relation between α and attaching folic acid to micelles as a targeting moiety. Nonetheless, this cannot be concluded from this study, since more experiments are needed to investigate this issue and decide on the significance of the differences by statistical tests. Yet, since the folic acid molecule is small, it may not have a significant effect on the acoustic properties of the micelles.

2. Beta (β):

The results obtained for the second constant (β) are shown in Table (C-2) in the Appendix and in Figure (5-2) where the results are the average \pm standard deviation of the replicates indicated in Table B.1 in the Appendix.

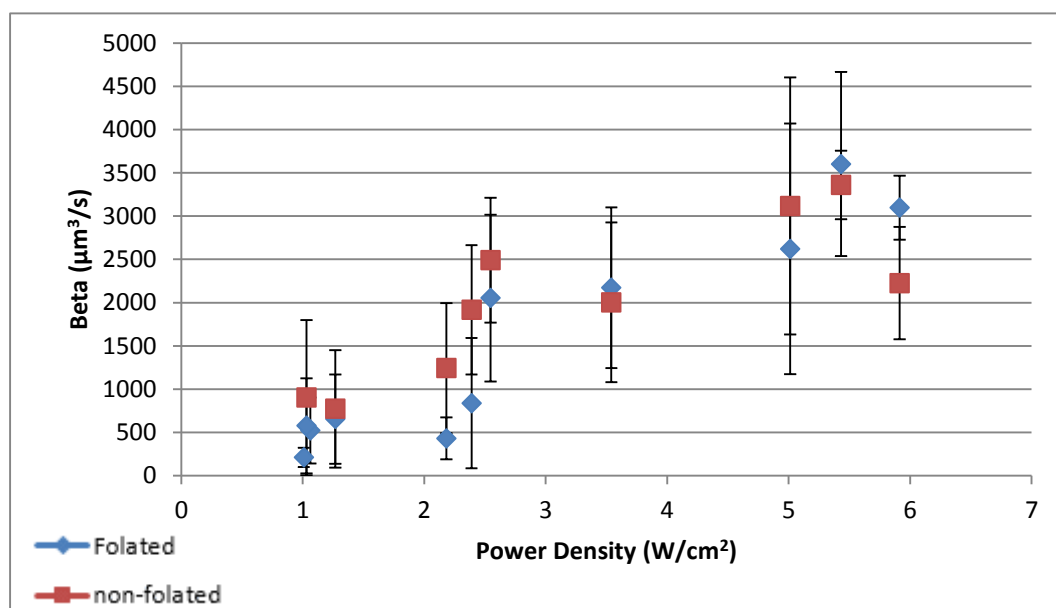


Figure 5-2: The relation between the power density and the Beta parameter which is related to the rate of micellar re-assembly.

β is the micelle re-assembly parameter. This temperature-dependent parameter indicates how destroyed micelles re-assemble back into new micelles. Based on the model equations, any increase in this parameter means that the number of micelles (M) increases with time. This can be explained as follows: since most of the micelles are destroyed rapidly, the re-assembly process increases proportionally. Furthermore, as mentioned in Chapter 2, micelle destruction and re-assembly happen simultaneously during insonation, in a competing fashion.

The results show that this parameter changes proportionally with power density. Since, at lower power densities there are fewer cavitation events, there will be less microstreaming and lower incidences of shock waves, hence the amount of micelles destroyed is lower compared with that at higher power densities. Thus, re-assembly at lower intensities will also be lower. The results presented in the graph confirm this relation. Also, the difference between folated and non-folated micelles was found to be small, possibly for the same reason previously discussed regarding α .

3. Lambda (λ):

The results obtained for the third constant (λ) are summarized in Table (C-3) in the Appendix and Figure (5-3), shown below where results are the average \pm standard deviation of the replicates indicated in Table B.1 in the Appendix.

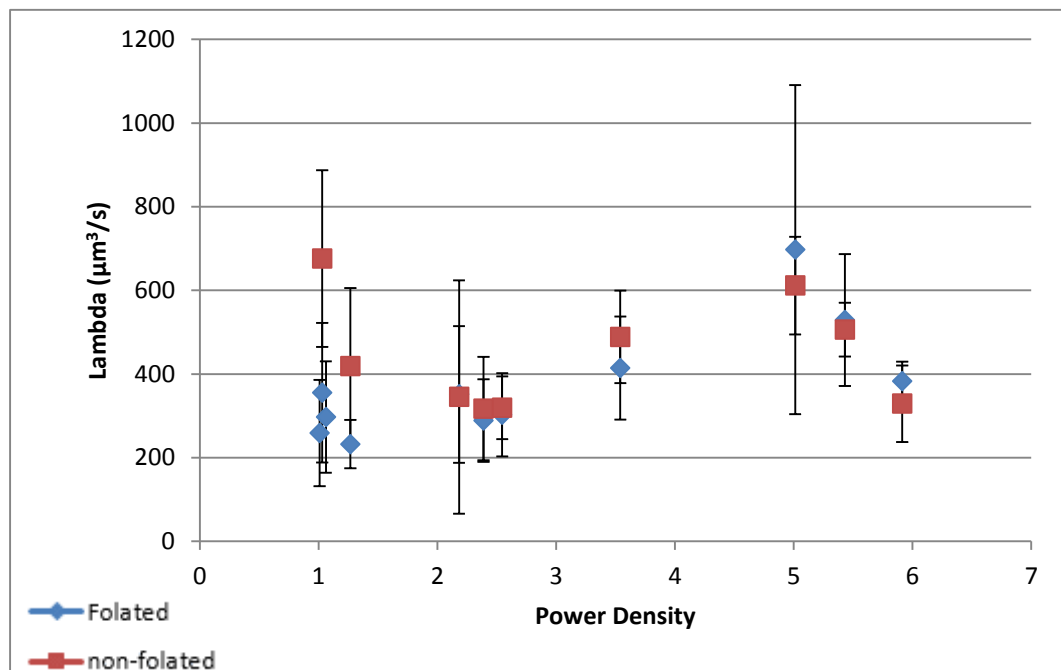


Figure 5-3: The relation between power density and its effect on the drug re-encapsulation parameter lambda.

λ is the drug encapsulation parameter, which is related to the rapid initial phase after insonation. This parameter is also temperature-dependent, and describes how this phase quickly ends, meaning that a long initial phase indicates a small value of λ and vice versa.

The results show fluctuations in the value for λ within a small range of values, which indicates that the value of λ is almost constant. Hence, λ does not seem to be correlated to the power density. Also the comparison between folated and non-targeted micelles shows that the behavior of λ is similar for both. It was hypothesized that the higher the ultrasonic intensity, the higher the scatter of the destroyed micelles (i.e. as the micelles dissociate, their polymers possibly travel further distances when the insonation is done at high power densities) [10]. Thus, at higher power densities, the reassembly process should take a longer period. However, based on the results of the constant λ , which quantifies the drug encapsulation rate, it appears that the rate is almost constant regardless of the US intensity. Hence, this hypothesis does not appear to be correct, or the sample used in this work is too low to conclude this which requires more investigation.

5.2. Tukey-Kramer's test and T-test for result analysis

The Tukey method is a statistical multiple comparison test used to determine if individual means are significantly different from a set of means [87]. The test makes use of the average of each set of data, calculates the difference between any pair of these averages, and compares it to the standard error. If the difference is less than the standard error, the means are assumed to have no significant difference; otherwise, the means are considered statistically significantly different. For unequal sample sizes, a modification of this method, introduced by Clyde Kramer in 1956 [88], can be used, and the test is referred to as the *Tukey Kramer test*.

In our work, the Tukey-Kramer test (with 95% confidence intervals) was performed for the means of every constant obtained for every power density, to decide if the results were significant (i.e., if *Alpha* and *Beta* are significantly increasing with the power density, and if *Lambda* does not change with power density). The results of this test for every parameter are presented in Tables (5-1) to (5.6). The upper part of these tables indicates the minimum significant difference (standard error), while the bottom part shows the results for the actual difference between each set of data. As for

the shaded cells within the tables, they indicate the sets of data that are significantly different.

The power density used in the experiments was changed by varying the voltage input of the US probe. Then the voltage values were converted to power density, as indicated in Appendix B.

Table 5-1: Tukey-Kramer test results for *Alpha* Folated-P105.

Power Density	1.009	1.062	1.030	1.267	2.183	2.389	2.546	3.540	5.013	5.432	5.914
1.009	-	0.0153	0.0169	0.0221	0.0191	0.0169	0.0175	0.0175	0.0182	0.0169	0.0247
1.062	0.0089	-	0.0166	0.0219	0.0189	0.0166	0.0172	0.0172	0.0179	0.0166	0.0245
1.030	0.0105	0.0016	-	0.0230	0.0202	0.0180	0.0186	0.0186	0.0193	0.0180	0.0255
1.267	0.0088	0.0177	0.0193	-	0.0247	0.0230	0.0234	0.0234	0.0240	0.0230	0.0292
2.183	0.0165	0.0254	0.0271	0.0077	-	0.0202	0.0207	0.0207	0.0213	0.0202	0.0271
2.389	0.0262	0.0351	0.0368	0.0174	0.0097	-	0.0186	0.0186	0.0193	0.0180	0.0255
2.546	0.0270	0.0359	0.0375	0.0182	0.0105	0.0008	-	0.0191	0.0198	0.0186	0.0259
3.540	0.0373	0.0462	0.0479	0.0285	0.0208	0.0111	0.0103	-	0.0198	0.0186	0.0259
5.013	0.0376	0.0465	0.0482	0.0289	0.0211	0.0114	0.0106	0.0003	-	0.0193	0.0264
5.432	0.0405	0.0494	0.0511	0.0317	0.0240	0.0143	0.0135	0.0032	0.0029	-	0.0255
5.914	0.0425	0.0514	0.0531	0.0337	0.0260	0.0163	0.0155	0.0052	0.0049	0.0020	-

Table 5-2: Tukey-Kramer test results for *Beta* Folated-P105.

Power Density	1.009	1.062	1.030	1.267	2.183	2.389	2.546	3.540	5.013	5.432	5.914
1.009	-	1058	1165.5	1526	1321.5	1165.5	1206.4	1206.4	1257	1165.5	1706.1
1.062	503.4	-	1146.1	1511	1304.5	1146.1	1187.7	1187.7	1239.1	1146.1	1692.9
1.030	477.6	981	-	1588	1393	1245.9	1284.3	1284.3	1331.9	1245.9	1762
1.267	926.8	1430.2	449.2	-	1706.1	1588.2	1618.5	1618.5	1656.6	1588.2	2018.6
2.183	1045.4	1548.8	567.8	118.6	-	1393	1427.4	1427.4	1470.4	1393	1868.9
2.389	2260.9	2764.3	1783.2	1334	1215.5	-	1284.3	1284.3	1331.9	1245.9	1762
2.546	2666.3	3170	2188.7	1740	1620.9	405.5	-	1321.5	1367.9	1284.3	1789.3
3.540	2444.1	2947.5	1966.5	1517	1398.7	183.26	222.22	-	1367.9	1284.3	1789.3
5.013	2521.3	3024.7	2043.7	1595	1475.9	260.44	145.04	77.18	-	1331.9	1823.8
5.432	2575.6	3079	2098	1649	1530.2	314.76	90.72	131.5	54.32	-	1762
5.914	2886.7	3390	2409	1960	1841.2	625.8	220.31	442.5	365.4	311.03	-

Table 5-3: Tukey-Kramer test results for *Lambda* Folated-P105.

Power Density	1.009	1.062	1.030	1.267	2.183	2.389	2.546	3.540	5.013	5.432	5.914
1.009	-	228.85	252.08	330.05	285.83	252.08	260.93	260.93	271.88	252.08	369.01
1.062	146.46	-	247.89	326.86	282.14	247.89	256.88	256.88	268.00	247.89	366.16
1.030	314.53	168.08	-	343.52	301.29	269.48	277.78	277.78	288.09	269.48	381.11
1.267	31.51	114.95	283.03	-	369.01	343.53	350.07	350.07	358.31	343.53	436.61
2.183	80.07	226.53	394.60	111.58	-	301.29	308.73	308.73	318.04	301.29	404.23
2.389	93.96	240.41	408.50	125.46	13.88	-	277.78	277.78	288.09	269.48	381.11
2.546	31.29	177.75	345.80	62.80	48.78	62.67	-	285.83	295.86	277.78	387.02
3.540	150.38	296.84	464.90	181.89	70.31	56.43	119.09	-	295.86	277.78	387.02
5.013	26.99	173.44	341.50	58.49	53.08	66.97	4.30	123.40	-	288.09	394.48
5.432	85.62	232.08	400.20	117.13	5.55	8.34	54.33	64.76	58.63	-	381.11
5.914	123.92	270.38	438.50	155.43	43.85	29.96	92.63	26.46	96.93	38.30	-

The previous three tables indicate the significant difference for the data concerning the folated micelle experiments. As shown in Table (C-1) and Figure (5-1) *Alpha* exhibited an increasing trend as the power density was increased. The Tukey-Kramer test results show that only about 50% of the data is significant, mainly the differences between high and low power densities. A similar correlation was observed for the *Beta* parameter (Table (C-2) and Figure (5-2)).

This can be explained by referring to Figures (5.1) and (5.2) and analyzing the experimental procedure followed for data collection. If the power densities are examined, it is clear that the data can be divided into two regions. The first region is the low power density region. Within this region, the steps used to increase the power densities were very small; hence, the data was condensed between power densities 1 W/cm² and 3 W/cm². The second region within those two graphs lies between 3 and 6 W/cm². Unlike the first region, here the power density is increased in bigger increments. This results in statistically significant differences between the pairs from the first and second regions, while no statistically significant differences can be deduced between pairs of the same region, and this is what the results clearly suggest.

The constant *lambda*, however does not change with power density, and this was confirmed by the Tukey-Kramer test (Table 5-3). As can be observed, the differences are not significant, except for one point (at 1.030 W/cm²). By examining the first three power densities used for the folated micelles (1.009, 1.062, 1.030) W/cm², we can assume they are almost the same. So, we expect to have almost the same results from the Tukey-Kramer test for the three of them. However, the data at power density

1.030 W/cm² showed different outcomes than the other two. This might imply a possible experimental outlier in the data collected. Nonetheless, the general behavior of lambda does not seem to significantly change with increasing power densities.

Similarly to what was done with the folated micelles' data, the Tukey-Kramer test was done for the three constants obtained for data collected in Dox release experiments from un-folated micelles, to check for significant differences in the data. The results are presented in the following three Tables 5-4, 5-5 and 5.6.

Table 5-4: Tukey Kramer test results for *Alpha* P105.

Power Density	1.030	1.267	2.183	2.389	2.546	3.540	5.013	5.432	5.914
1.030	-	0.01472	0.01472	0.01472	0.01472	0.01472	0.01544	0.01472	0.01472
1.267	0.01916	-	0.01472	0.01472	0.01472	0.01472	0.01544	0.01472	0.01472
2.183	0.02021	0.00105	-	0.01472	0.01472	0.01472	0.01544	0.01472	0.01472
2.389	0.01021	0.00896	0.01001	-	0.01472	0.01472	0.01544	0.01472	0.01472
2.546	0.00340	0.02256	0.02361	0.01361	-	0.01472	0.01544	0.01472	0.01472
3.540	0.00472	0.02389	0.02494	0.01493	0.00132	-	0.01544	0.01472	0.01472
5.013	0.01126	0.03042	0.03147	0.02147	0.00786	0.00654	-	0.01544	0.01544
5.432	0.01485	0.03401	0.03506	0.02505	0.01145	0.01012	0.00359	-	0.01472
5.914	0.01282	0.03198	0.03303	0.02303	0.00942	0.00810	0.00156	0.00203	-

Table 5-5: Tukey Kramer test results for *Beta* P105.

Power Density	1.030	1.267	2.183	2.389	2.546	3.540	5.013	5.432	5.914
1.030	-	1609.4	1609.4	1609.39	1609.4	1609.39	1687.94	1609.39	1609.4
1.267	1134.4	-	1609.4	1609.39	1609.4	1609.39	1687.94	1609.39	1609.4
2.183	890.7	243.69	-	1609.39	1609.4	1609.39	1687.94	1609.39	1609.4
2.389	222.48	1356.8	1113.2	-	1609.4	1609.39	1687.94	1609.39	1609.4
2.546	265.39	869	625.3	487.9	-	1609.39	1687.94	1609.39	1609.4
3.540	309.15	1443.5	1199.8	86.66	574.5	-	1687.94	1609.39	1609.4
5.013	982.4	2116.8	1873.1	760	1247.8	673.3	-	1687.94	1687.9
5.432	1452.6	2586.9	2343.3	1230.1	1718	1143.4	470.1	-	1609.4
5.914	1323.4	2457.8	2214.1	1100.9	1588.8	1014.3	341	129.15	-

Table 5-6: Tukey Kramer test results for *Lambda* P105.

Power Density	1.030	1.267	2.183	2.389	2.546	3.540	5.013	5.432	5.914
1.030	-	284.56	284.56	284.56	284.56	284.56	298.45	284.56	284.56
1.267	176.99	-	284.56	284.56	284.56	284.56	298.45	284.56	284.56
2.183	282.40	105.40	-	284.56	284.56	284.56	298.45	284.56	284.56
2.389	159.75	17.25	122.65	-	284.56	284.56	298.45	284.56	284.56
2.546	9.78	186.77	292.18	169.53	-	284.56	298.45	284.56	284.56
3.540	11.79	188.79	294.19	171.54	2.01	-	298.45	284.56	284.56
5.013	16.12	160.88	266.28	143.63	25.90	27.91	-	298.45	298.45
5.432	89.67	87.32	192.72	70.07	99.45	101.47	73.56	-	284.56
5.914	346.80	169.81	64.41	187.06	356.60	358.60	330.70	257.13	-

The results from the above tables indicate the same observations for *Alpha*. However, for *Beta*, significant differences are expected to be the general trend, yet the table shows opposing behavior. There seems to be not much significance between the data points even between low and high power densities. This, compared to the Beta tables obtained for the folated micelles, might suggest inconsistency in the data collected which might be due to experimental errors. In general, Beta should exhibit a significant increasing behavior as the power density increases, which is not supported by the obtained results. As for *Lambda*, the results seem to be more supportive of the expected behavior which is assumed to be constant regardless of the power density. From the tables above, the results for this parameter seem to be more accurate as the significance degree is low which suggests a constant behavior.

The results were further analyzed to compare the three parameters for folated and non-folated micelles. This comparison was done by running a T-test that effectively measures the P-value which quantifies the existence of a significant difference between two groups of data. The test constraint was set at a 95% confidence level which means if the P-value was less than 0.05, then the data had a significant difference. As shown in the following table, there is no significant difference between the two types of micelles.

Table 5-7: T-test for the parameters in order to get the P-values

	Alpha	Beta	Lambda
P-value	0.664	0.666	0.443

Chapter 6 : Conclusion and Recommendation

6.1. Conclusion

In this work, a DDS composed of micelles as carriers and US as a trigger mechanism were studied to investigate the relation between drug release and power density from folated and non-folated micelles. Also, the effect of US on cellular uptake was reviewed and the advantages of using this DDS were asserted throughout this work. However, the main purpose of the work was to model the kinetics of release from those two types of carriers caused by the cavitation phenomenon associated with US and microbubbles.

The results were obtained using MATLAB software, which was used to program and model the release and re-encapsulation processes when US was used to release Dox from micelles. Three constants (α , β , λ) were regressed using this model. Then they were studied as a function of power density for the two types of micelles. The statistical significance of the results was assessed using the Tukey-Kramer statistical test. Constant α , which quantifies the rate of micellar destruction, and constant β , which measures the micelles' reassembly rate, were found to increase with increasing power density, albeit at different rates. Constant λ , which is related to the re-encapsulation of the drug in the micelles, was found to be constant with power density, which suggests that the re-encapsulation is independent of the power density used. The significance of the results obtained in this study was assessed using the Tukey-Kramer statistical test. For *alpha* and *beta* constants, we could observe significant differences for different power densities, while *lambda* seems to be constant.

A comparison between the results of folated and non-folated micelles was also conducted to examine the difference between both carriers. This comparison is critical as it signifies the difference in release behavior between two carriers that have the potential to be employed in DDS. According to the results obtained, it was found that both types of micelles behave similarly and there is no significant difference between them. This suggests that both of them can be used as carriers from which drug release can be triggered using ultrasound. Because of this, it can be said that the objectives of this study were successfully achieved.

6.2. Recommendations

As seen so far, the work has potential and could be an important addition to the literature. However, below are some recommendations that might help improve the results and analysis. First, any experimental work is subjected to several sources of error. In this case, the human error is probably significant, since many of the parameters were controlled manually. For example, the US turning *on* and *off* was done manually, so many of the readings did not overlap. This presented a challenge in calculating the average of the several runs, a process that was required to do the calculation for the constants.

Second, the denoising process was also done manually which may have caused some loss of valuable data. A way to overcome this is through the use of more accurate and specialized software, such as automated wavelet processing software or more optimized methods. Furthermore, other models and optimization techniques (e.g. the Gauss-Newton method and Gradient descent algorithm) can be used to achieve more accurate results.

Moreover, the data supplied for modeling had some inconsistencies that might be regarded as outliers. Since the number of data points used is not large enough, an outlier will definitely affect the model's behavior, as was discussed in the Results section. For example, the data collected for the power density equivalent to 140 V seemed to be out of the trend. So, it is recommended that the readings for those points be repeated and averaged as this will lead to more accurate results.

Also, it is believed that more data collection in this field may open the doors for further investigation. For example, if more data was collected to investigate the relation between release and the *alpha* parameter, it is believed that a more defined correlation between them could be observed.

References

- [1] J. S. Bertram, "The molecular biology of cancer," *Mol Aspects Med*, vol. 21, pp. 167-223, Dec 2000.
- [2] G.-J. J. Hong-Qiang Wang, Chunhou Zheng, "Biology-constrained gene expression discretization for cancer classification," *Neurocomputing*, vol. 145, pp. 30-36, 2014.
- [3] A. Jemal, F. Bray, M. M. Center, J. Ferlay, E. Ward, and D. Forman, "Global cancer statistics," *CA Cancer J Clin*, vol. 61, pp. 69-90, Mar-Apr 2011.
- [4] D. M. Parkin, F. Bray, J. Ferlay, and P. Pisani, "Global cancer statistics, 2002," *CA Cancer J Clin*, vol. 55, pp. 74-108, Mar-Apr 2005.
- [5] K. Biswanath, "Doxorubicin-intercalated nano-hydroxyapatite drug-delivery system for liver cancer: An animal model," *Ceramics International*, vol. 39, pp. 9557-9566, December 2013 2013.
- [6] Y. Cheng, R. A. Morshed, B. Auffinger, A. L. Tobias, and M. S. Lesniak, "Multifunctional nanoparticles for brain tumor imaging and therapy," *Adv Drug Deliv Rev*, Sep 20 2013.
- [7] H. Gandhi, V. B. Patel, N. Mistry, N. Patni, J. Nandania, and R. Balaraman, "Doxorubicin mediated cardiotoxicity in rats: Protective role of felodipine on cardiac indices," *Environ Toxicol Pharmacol*, vol. 36, pp. 787-95, Nov 2013.
- [8] F. Cuomo, M. Mosca, S. Murgia, P. Avino, A. Ceglie, and F. Lopez, "Evidence for the role of hydrophobic forces on the interactions of nucleotide-monophosphates with cationic liposomes," *J Colloid Interface Sci*, vol. 410, pp. 146-51, Nov 15 2013.
- [9] G. A. Hussein, D. Stevenson-Abouelnasr, W. G. Pitt, K. T. Assaleh, L. O. Farahat, and J. Fahadi, "Kinetics and Thermodynamics of Acoustic Release of Doxorubicin from Non-stabilized polymeric Micelles," *Colloids Surf A Physicochem Eng Asp*, vol. 359, pp. 18-24, Apr 20 2010.
- [10] D. Stevenson-Abouelnasr, G. A. Hussein, and W. G. Pitt, "Further investigation of the mechanism of Doxorubicin release from P105 micelles using kinetic models," *Colloids Surf B Biointerfaces*, vol. 55, pp. 59-66, Mar 15 2007.
- [11] G. A. Hussein, R. I. El-Fayoumi, K. L. O'Neill, N. Y. Rapoport, and W. G. Pitt, "DNA damage induced by micellar-delivered doxorubicin and ultrasound: comet assay study," *Cancer Lett*, vol. 154, pp. 211-6, Jun 30 2000.
- [12] G. Gaucher, M. H. Dufresne, V. P. Sant, N. Kang, D. Maysinger, and J. C. Leroux, "Block copolymer micelles: preparation, characterization and application in drug delivery," *J Control Release*, vol. 109, pp. 169-88, Dec 5 2005.
- [13] S. R. Croy and G. S. Kwon, "Polymeric micelles for drug delivery," *Curr Pharm Des*, vol. 12, pp. 4669-84, 2006.
- [14] G. A. Hussein and W. G. Pitt, "The use of ultrasound and micelles in cancer treatment," *J Nanosci Nanotechnol*, vol. 8, pp. 2205-15, May 2008.

- [15] G. A. Hussein, D. Velluto, L. Kherbeck, W. G. Pitt, J. A. Hubbell, and D. A. Christensen, "Investigating the acoustic release of doxorubicin from targeted micelles," *Colloids Surf B Biointerfaces*, vol. 101, pp. 153-5, Jan 1 2013.
- [16] A. Beduneau, P. Saulnier, and J. P. Benoit, "Active targeting of brain tumors using nanocarriers," *Biomaterials*, vol. 28, pp. 4947-67, Nov 2007.
- [17] G. A. Hussein, G. D. Myrup, W. G. Pitt, D. A. Christensen, and N. Y. Rapoport, "Factors affecting acoustically triggered release of drugs from polymeric micelles," *J Control Release*, vol. 69, pp. 43-52, Oct 3 2000.
- [18] M. A. Diaz de la Rosa, G. A. Hussein, and W. G. Pitt, "Mathematical modeling of microbubble cavitation at 70 kHz and the importance of the subharmonic in drug delivery from micelles," *Ultrasonics*, vol. 53, pp. 97-110, Jan 2013.
- [19] S. E. Ahmed, A. M. Martins, and G. A. Hussein, "The use of ultrasound to release chemotherapeutic drugs from micelles and liposomes," *J Drug Target*, pp. 1-27, Sep 9 2014.
- [20] G. A. Hussein, F. S. Mjalli, W. G. Pitt, and N. Abdel-Jabbar, "Using artificial neural networks and model predictive control to optimize acoustically assisted Doxorubicin release from polymeric micelles," *Technol Cancer Res Treat*, vol. 8, pp. 479-88, Dec 2009.
- [21] G. H. John D. Pruitt, Natalya Rapoport, and William G. Pitt, "Stabilization of Pluronic P-105 Micelles with an Interpenetrating Network of N,N-Diethylacrylamide," *Macromolecules* vol. 33, 2000.
- [22] G. A. Hussein, M. A. Diaz de la Rosa, T. Gabuji, Y. Zeng, D. A. Christensen, and W. G. Pitt, "Release of doxorubicin from unstabilized and stabilized micelles under the action of ultrasound," *J Nanosci Nanotechnol*, vol. 7, pp. 1028-33, Mar 2007.
- [23] G. A. Hussein, W. G. Pitt, D. A. Christensen, and D. J. Dickinson, "Degradation kinetics of stabilized Pluronic micelles under the action of ultrasound," *J Control Release*, vol. 138, pp. 45-8, Aug 19 2009.
- [24] B. J. Staples, W. G. Pitt, B. L. Roeder, G. A. Hussein, D. Rajeev, and G. B. Schaalje, "Distribution of doxorubicin in rats undergoing ultrasonic drug delivery," *J Pharm Sci*, vol. 99, pp. 3122-31, Jul 2010.
- [25] G. A. Hussein, D. A. Christensen, N. Y. Rapoport, and W. G. Pitt, "Ultrasonic release of doxorubicin from Pluronic P105 micelles stabilized with an interpenetrating network of N,N-diethylacrylamide," *J Control Release*, vol. 83, pp. 303-5, Oct 4 2002.
- [26] N. M. A.-J. Ghaleb A. Hussein, Farouq S. Mjalli, William G. Pitt, Ala'a Al-Mousa, "Optimizing the use of ultrasound to deliver chemotherapeutic agents to cancer cells from polymeric micelles," *Journal of the Franklin Institute*, vol. 348, pp. 1276-1284, 2010.
- [27] M. A. Diaz de la Rosa, G. A. Hussein, and W. G. Pitt, "Comparing microbubble cavitation at 500 kHz and 70 kHz related to micellar drug delivery using ultrasound," *Ultrasonics*, vol. 53, pp. 377-86, Feb 2013.
- [28] W. G. Pitt, G. A. Hussein, and B. J. Staples, "Ultrasonic drug delivery--a general review," *Expert Opin Drug Deliv*, vol. 1, pp. 37-56, Nov 2004.

- [29] S. Mitragotri, "Healing sound: the use of ultrasound in drug delivery and other therapeutic applications," *Nat Rev Drug Discov*, vol. 4, pp. 255-60, Mar 2005.
- [30] G. Hussein, "Kinetics of ultrasonic release of doxorubicin from pluronic P105 micelles," *Colloids Surf B Biointerfaces*, vol. 24, pp. 253-264, April 2002.
- [31] A. Schroeder, J. Kost, and Y. Barenholz, "Ultrasound, liposomes, and drug delivery: principles for using ultrasound to control the release of drugs from liposomes," *Chem Phys Lipids*, vol. 162, pp. 1-16, Nov 2009.
- [32] G. A. Hussein and W. G. Pitt, "Micelles and nanoparticles for ultrasonic drug and gene delivery," *Adv Drug Deliv Rev*, vol. 60, pp. 1137-52, Jun 30 2008.
- [33] G. A. Hussein, M. A. Diaz de la Rosa, E. S. Richardson, D. A. Christensen, and W. G. Pitt, "The role of cavitation in acoustically activated drug delivery," *J Control Release*, vol. 107, pp. 253-61, Oct 3 2005.
- [34] L. K. Ghaleb A. Husseni, William G. Pitt, Jeffrey A. Hubbell, Douglas A. Christensen and Diana Velluto, "Kinetics of ultrasonic drug delivery from targeted micelles," *Journal of Nanoscience and Nanotechnology*, vol. 14, pp. 1-6, 2014.
- [35] S. B. Stringham, M. A. Viskovska, E. S. Richardson, S. Ohmine, G. A. Hussein, B. K. Murray, and W. G. Pitt, "Over-pressure suppresses ultrasonic-induced drug uptake," *Ultrasound Med Biol*, vol. 35, pp. 409-15, Mar 2009.
- [36] D. O. Draper, J. C. Castel, and D. Castel, "Rate of temperature increase in human muscle during 1 MHz and 3 MHz continuous ultrasound," *J Orthop Sports Phys Ther*, vol. 22, pp. 142-50, Oct 1995.
- [37] M. de Smet, S. Langereis, S. van den Bosch, and H. Grull, "Temperature-sensitive liposomes for doxorubicin delivery under MRI guidance," *J Control Release*, vol. 143, pp. 120-7, Apr 2 2009.
- [38] A. Gasselhuber, M. R. Dreher, F. Rattay, B. J. Wood, and D. Haemmerich, "Comparison of conventional chemotherapy, stealth liposomes and temperature-sensitive liposomes in a mathematical model," *PLoS One*, vol. 7, p. e47453, 2012.
- [39] S. M. Park, M. S. Kim, S. J. Park, E. S. Park, K. S. Choi, Y. S. Kim, and H. R. Kim, "Novel temperature-triggered liposome with high stability: formulation, in vitro evaluation, and in vivo study combined with high-intensity focused ultrasound (HIFU)," *J Control Release*, vol. 170, pp. 373-9, Sep 28 2013.
- [40] C. D. Arvanitis, M. Bazan-Peregrino, B. Rifai, L. W. Seymour, and C. C. Coussios, "Cavitation-enhanced extravasation for drug delivery," *Ultrasound Med Biol*, vol. 37, pp. 1838-52, Nov 2011.
- [41] M. Abdullah, "Polymeric Micelles for Drug Targeting," *Journal of Drug Targeting*, vol. 15, pp. 553-584, 2007.
- [42] C. Oerlemans, W. Bult, M. Bos, G. Storm, J. F. Nijsen, and W. E. Hennink, "Polymeric micelles in anticancer therapy: targeting, imaging and triggered release," *Pharm Res*, vol. 27, pp. 2569-89, Dec 2010.
- [43] D. M. Webster, P. Sundaram, and M. E. Byrne, "Injectable nanomaterials for drug delivery: carriers, targeting moieties, and therapeutics," *Eur J Pharm Biopharm*, vol. 84, pp. 1-20, May 2013.

- [44] J. D. Byrne, T. Betancourt, and L. Brannon-Peppas, "Active targeting schemes for nanoparticle systems in cancer therapeutics," *Adv Drug Deliv Rev*, vol. 60, pp. 1615-26, Dec 14 2008.
- [45] Y. Lu and P. S. Low, "Folate-mediated delivery of macromolecular anticancer therapeutic agents," *Adv Drug Deliv Rev*, vol. 54, pp. 675-93, Sep 13 2002.
- [46] V. Torchilin, "Drug Targeting," *European Journal of Pharmaceutical Sciences*, vol. 11, pp. S81-S91, October 2000.
- [47] D. R. Burton, "Phage display," *Immunotechnology*, vol. 1, pp. 87-94, Aug 1995.
- [48] M. K. Yu, J. Park, and S. Jon, "Targeting strategies for multifunctional nanoparticles in cancer imaging and therapy," *Theranostics*, vol. 2, pp. 3-44, 2012.
- [49] K. S. Lam, M. Lebl, and V. Krchnak, "The "One-Bead-One-Compound" Combinatorial Library Method," *Chem Rev*, vol. 97, pp. 411-448, Apr 1 1997.
- [50] O. H. Aina, R. Liu, J. L. Sutcliffe, J. Marik, C. X. Pan, and K. S. Lam, "From combinatorial chemistry to cancer-targeting peptides," *Mol Pharm*, vol. 4, pp. 631-51, Sep-Oct 2007.
- [51] M. Talelli, S. Oliveira, C. J. Rijcken, E. H. Pieters, T. Etrych, K. Ulbrich, R. C. van Nostrum, G. Storm, W. E. Hennink, and T. Lammers, "Intrinsically active nanobody-modified polymeric micelles for tumor-targeted combination therapy," *Biomaterials*, vol. 34, pp. 1255-60, Jan 2013.
- [52] R. K. F. X. Gu, A. Z. Wang, F. Alexis, E. L.-Nissenbaum, S. Hong, R. S. Langer, O. C. Farokhzad, "Targeted nanoparticles for cancer therapy," *Nano Today*, vol. 2, pp. 14-21, June 2007.
- [53] M. N. N. Abdulla, A. Markowitz, ""Rituximab"," *Wolters Kluwer Health Adis Internatrional*, April 2012.
- [54] S. Goel, J. Chirgwin, P. Francis, R. Stuart-Harris, J. Dewar, L. Mileskin, R. Snyder, M. Michael, and B. Koczwara, "Rational use of trastuzumab in metastatic and locally advanced breast cancer: implications of recent research," *Breast*, vol. 20, pp. 101-10, Apr 2011.
- [55] L. M. Randall and B. J. Monk, "Bevacizumab toxicities and their management in ovarian cancer," *Gynecol Oncol*, vol. 117, pp. 497-504, Jun 2010.
- [56] T. Shih and C. Lindley, "Bevacizumab: an angiogenesis inhibitor for the treatment of solid malignancies," *Clin Ther*, vol. 28, pp. 1779-802, Nov 2006.
- [57] J. C. S. Goel, P. Francis, R. Stuart-Harris, J. Dewar, L. Mileskin, R. Snyder, M. Michael, B. Koczwara, "Rational use of trastuzumab in metastatic and locally advanced breast cancer: Implications of recent research," *The Breast*, vol. 20, pp. 398-400, 2011.
- [58] S. Shigdar, L. Qiao, S. F. Zhou, D. Xiang, T. Wang, Y. Li, L. Y. Lim, L. Kong, L. Li, and W. Duan, "RNA aptamers targeting cancer stem cell marker CD133," *Cancer Lett*, vol. 330, pp. 84-95, Mar 1 2013.
- [59] L. Cerchia and V. de Franciscis, "Targeting cancer cells with nucleic acid aptamers," *Trends Biotechnol*, vol. 28, pp. 517-25, Oct 2010.

- [60] Z. Shen, Y. Li, K. Kohama, B. Oneill, and J. Bi, "Improved drug targeting of cancer cells by utilizing actively targetable folic acid-conjugated albumin nanospheres," *Pharmacol Res*, vol. 63, pp. 51-8, Jan 2011.
- [61] J. Ai, Y. Xu, D. Li, Z. Liu, and E. Wang, "Folic acid as delivery vehicles: targeting folate conjugated fluorescent nanoparticles to tumors imaging," *Talanta*, vol. 101, pp. 32-7, Nov 15 2012.
- [62] U.S. National Institutes of Health. "Clinical studies of human participants conducted around the world". Internet: <https://clinicaltrials.gov/>, Feb. 2000 [Dec. 2, 2014].
- [63] N. Munshi, N. Rapoport, and W. G. Pitt, "Ultrasonic activated drug delivery from Pluronic P-105 micelles," *Cancer Lett*, vol. 118, pp. 13-9, Sep 16 1997.
- [64] A. Marin, H. Sun, G. A. Hussein, W. G. Pitt, D. A. Christensen, and N. Y. Rapoport, "Drug delivery in pluronic micelles: effect of high-frequency ultrasound on drug release from micelles and intracellular uptake," *J Control Release*, vol. 84, pp. 39-47, Nov 7 2002.
- [65] A. Marin, M. Muniruzzaman, and N. Rapoport, "Acoustic activation of drug delivery from polymeric micelles: effect of pulsed ultrasound," *J Control Release*, vol. 71, pp. 239-49, Apr 28 2001.
- [66] K. Tachibana, T. Uchida, K. Tamura, H. Eguchi, N. Yamashita, and K. Ogawa, "Enhanced cytotoxic effect of Ara-C by low intensity ultrasound to HL-60 cells," *Cancer Lett*, vol. 149, pp. 189-94, Feb 28 2000.
- [67] N. Yamashita, K. Tachibana, K. Ogawa, N. Tsujita, and A. Tomita, "Scanning electron microscopic evaluation of the skin surface after ultrasound exposure," *Anat Rec*, vol. 247, pp. 455-61, Apr 1997.
- [68] K. Tachibana, T. Uchida, K. Ogawa, N. Yamashita, and K. Tamura, "Induction of cell-membrane porosity by ultrasound," *Lancet*, vol. 353, p. 1409, Apr 24 1999.
- [69] R. K. Schlicher, J. D. Hutcheson, H. Radhakrishna, R. P. Apkarian, and M. R. Prausnitz, "Changes in cell morphology due to plasma membrane wounding by acoustic cavitation," *Ultrasound Med Biol*, vol. 36, pp. 677-92, Apr 2010.
- [70] R. K. Schlicher, H. Radhakrishna, T. P. Tolentino, R. P. Apkarian, V. Zarnitsyn, and M. R. Prausnitz, "Mechanism of intracellular delivery by acoustic cavitation," *Ultrasound Med Biol*, vol. 32, pp. 915-24, Jun 2006.
- [71] E. S. Richardson, W. G. Pitt, and D. J. Woodbury, "The role of cavitation in liposome formation," *Biophys J*, vol. 93, pp. 4100-7, Dec 15 2007.
- [72] Y. Zhou, R. E. Kumon, J. Cui, and C. X. Deng, "The size of sonoporation pores on the cell membrane," *Ultrasound Med Biol*, vol. 35, pp. 1756-60, Oct 2009.
- [73] J. Hauser, M. Ellisman, H. U. Steinau, E. Stefan, M. Dudda, and M. Hauser, "Ultrasound enhanced endocytotic activity of human fibroblasts," *Ultrasound Med Biol*, vol. 35, pp. 2084-92, Dec 2009.
- [74] B. D. Meijering, L. J. Juffermans, A. van Wamel, R. H. Henning, I. S. Zuhorn, M. Emmer, A. M. Versteilen, W. J. Paulus, W. H. van Gilst, K. Kooiman, N. de Jong, R. J. Musters, L. E. Deelman, and O. Kamp, "Ultrasound and

- microbubble-targeted delivery of macromolecules is regulated by induction of endocytosis and pore formation," *Circ Res*, vol. 104, pp. 679-87, Mar 13 2009.
- [75] M. Muniruzzaman, "Intracellular uptake of pluronic copolymer: effects of the aggregation state," *Colloids and Surfaces B: Biointerfaces*, vol. 25, pp. 233-241, 2002.
- [76] N. Rapoport, "Combined cancer therapy by micellar-encapsulated drug and ultrasound," *Int J Pharm*, vol. 277, pp. 155-62, Jun 11 2004.
- [77] N. Sheikov, N. McDannold, F. Jolesz, Y. Z. Zhang, K. Tam, and K. Hynynen, "Brain arterioles show more active vesicular transport of blood-borne tracer molecules than capillaries and venules after focused ultrasound-evoked opening of the blood-brain barrier," *Ultrasound Med Biol*, vol. 32, pp. 1399-409, Sep 2006.
- [78] B. Howard, Gao, Z., Lee, S. W., Seo, M. H., & Rapoport, N., "Ultrasound-enhanced chemotherapy of drug-resistant breast cancer tumors by micellar-encapsulated paclitaxel," *American Journal of Drug Delivery*, vol. 4, pp. 97-104, 2006
- [79] H. Zhang, H. Xia, J. Wang, and Y. Li, "High intensity focused ultrasound-responsive release behavior of PLA-b-PEG copolymer micelles," *J Control Release*, vol. 139, pp. 31-9, Oct 1 2009.
- [80] L. Chen, X. Sha, X. Jiang, Y. Chen, Q. Ren, and X. Fang, "Pluronic P105/F127 mixed micelles for the delivery of docetaxel against Taxol-resistant non-small cell lung cancer: optimization and in vitro, in vivo evaluation," *Int J Nanomedicine*, vol. 8, pp. 73-84, 2013.
- [81] M. Ugarenko, C. K. Chan, A. Nudelman, A. Rephaeli, S. M. Cutts, and D. R. Phillips, "Development of pluronic micelle-encapsulated doxorubicin and formaldehyde-releasing prodrugs for localized anticancer chemotherapy," *Oncol Res*, vol. 17, pp. 283-99, 2009.
- [82] J. L. Nelson, B. L. Roeder, J. C. Carmen, F. Roloff, and W. G. Pitt, "Ultrasonically activated chemotherapeutic drug delivery in a rat model," *Cancer Res*, vol. 62, pp. 7280-3, Dec 15 2002.
- [83] B. J. Staples, B. L. Roeder, G. A. Hussein, O. Badamjav, G. B. Schaalje, and W. G. Pitt, "Role of frequency and mechanical index in ultrasonic-enhanced chemotherapy in rats," *Cancer Chemother Pharmacol*, vol. 64, pp. 593-600, Aug 2009.
- [84] N. Y. Rapoport, D. A. Christensen, H. D. Fain, L. Barrows, and Z. Gao, "Ultrasound-triggered drug targeting of tumors in vitro and in vivo," *Ultrasonics*, vol. 42, pp. 943-50, Apr 2004.
- [85] H. Hasanzadeh, M. Mokhtari-Dizaji, S. Z. Bathaie, and Z. M. Hassan, "Effect of local dual frequency sonication on drug distribution from polymeric nanomicelles," *Ultrason Sonochem*, vol. 18, pp. 1165-71, Sep 2011.
- [86] G. Hussein, "Folated and Non-folatede Micelles Release Data", unpublished work. Utah, U.S.: University of Utah, 2012.
- [87] W. Dubitzky, Wolkenhauer, O., Cho, K.-H., Yokota, H., eds, "Tukey's Test " in *Encyclopedia of Systems Biology* W. Haynes, Ed.: Springer, 2013.

- [88] C. Y. Kramer, "Extension of multiple range tests to group means with unequal numbers of replications," *Biometrics*, vol. 12, pp. 307-310, 1956.

Appendix

A. Designed Modeling Program for MATLAB:

Table A-1: Script Part for the MATLAB Program.

```
% This program is designed for modeling of drug release data for a thesis work for
Rafeeq K Tanbour based on

% mathematical model proposed by Dr. Ghaleb Husseini and his research group.

% Program designed by:

% Rafeeq K. Tanbour & Mohamed El-Khodairy

% American University of Sharjah. 2014

% Mi : micelle fraction M with their group number i.

% Di : micelle Diameter with for every group.

% Ei : percentage of drug for every group.

% v: symbol used for every parameter where v(1) is alpha, v(2) is beta and v(3) is
lambda.

M1(1)=0.372;
M2(1)=0.226;
M3(1)=0.177;
M4(1)=0.135;
M5(1)=0.089;

D1=11.6;
D2=14.0;
D3=15.0;
D4=16.5;
D5=19.6;

D1cubed=1618;
D2cubed=2670;
D3cubed=3411;
D4cubed=4469;
D5cubed=6765;

DcubedT=D1cubed+D2cubed+D3cubed+D4cubed+D5cubed;
```

```

N=1;

E1(1)=0.2;

E2(1)=0.2;

E3(1)=0.2;

E4(1)=0.2;

E5(1)=0.2;

E(1)=1;

Vfp(1)=0;

dt=0.02; %interval

v=[0.04;330;100];

Ee=AvgDN';

% lower and upper limits

vlb=[0.001;150;50];

vub=[1;1000000;170500];

v=lsqcurvefit(@expected,v,[M1,M2,M3,M4,M5,E1,E2,E3,E4,E5],Ee,vlb,vub);

E=feval(@expected,v,M1,M2,M3,M4,M5,E1,E2,E3,E4,E5);

t=9.16:0.02:15; %initial to final time of triggering

plot(t,Ee,'ro')

hold on

plot(t,E)

xlabel('Time (sec)')

ylabel('Fraction Encapsulated')

format long

v=v'

```

Table A-2: Function Part for the MATLAB Program.

```
function E=expected(v,M1,M2,M3,M4,M5,E1,E2,E3,E4,E5)

M1(1)=0.372;
M2(1)=0.226;
M3(1)=0.177;
M4(1)=0.135;
M5(1)=0.089;

D1=11.6;
D2=14.0;
D3=15.0;
D4=16.5;
D5=19.6;

D1cubed=1618;
D2cubed=2670;
D3cubed=3411;
D4cubed=4469;
D5cubed=6765;

DcubedT=D1cubed+D2cubed+D3cubed+D4cubed+D5cubed;

N=1;

E1(1)=0.2;
E2(1)=0.2;
E3(1)=0.2;
E4(1)=0.2;
E5(1)=0.2;

E(1)=1;

Vfp(1)=0;

dt=0.02;

i=1;

for i=1:292 % Dimensions - 1
```

```

dM1(i)=(v(2)/D1cubed)*Vfp(i)-v(1)*D1*M1(i)*N;
dM2(i)=(v(2)/D2cubed)*Vfp(i)-v(1)*D2*M2(i)*N;
dM3(i)=(v(2)/D3cubed)*Vfp(i)-v(1)*D3*M3(i)*N;
dM4(i)=(v(2)/D4cubed)*Vfp(i)-v(1)*D4*M4(i)*N;
dM5(i)=(v(2)/D5cubed)*Vfp(i)-v(1)*D5*M5(i)*N;
dE1(i)=v(3)*(1-E(i))*M1(i)*(D1cubed/(D1*DcubedT))-v(1)*D1*N*E1(i);
dE2(i)=v(3)*(1-E(i))*M2(i)*(D2cubed/(D2*DcubedT))-v(1)*D2*N*E2(i);
dE3(i)=v(3)*(1-E(i))*M3(i)*(D3cubed/(D3*DcubedT))-v(1)*D3*N*E3(i);
dE4(i)=v(3)*(1-E(i))*M4(i)*(D4cubed/(D4*DcubedT))-v(1)*D4*N*E4(i);
dE5(i)=v(3)*(1-E(i))*M5(i)*(D5cubed/(D5*DcubedT))-v(1)*D5*N*E5(i);
M1(i+1)=M1(i)+dM1(i)*dt;
M2(i+1)=M2(i)+dM2(i)*dt;
M3(i+1)=M3(i)+dM3(i)*dt;
M4(i+1)=M4(i)+dM4(i)*dt;
M5(i+1)=M5(i)+dM5(i)*dt;
E1(i+1)=E1(i)+dE1(i)*dt;
E2(i+1)=E2(i)+dE2(i)*dt;
E3(i+1)=E3(i)+dE3(i)*dt;
E4(i+1)=E4(i)+dE4(i)*dt;
E5(i+1)=E5(i)+dE5(i)*dt;
Vfp(i+1)=1-
5*((M1(i)*D1cubed+M2(i)*D2cubed+M3(i)*D3cubed+M4(i)*D4cubed+M5(i)*D5cubed)/Dcub
edT);
i=i+1;
E(i)=E1(i)+E2(i)+E3(i)+E4(i)+E5(i);
end

```

B. Voltage to Power Density conversion

Table B-1: Voltage to Power Density conversion, and number of replicates for all points.

Voltage	Power Density	Number of replicates Folated-P105	Number of replicates P105
90	1.0086976	3	----
95	1.0621081	9	----
100	1.03041	9	6
105	1.26736	9	6
110	2.1827584	9	6
115	2.3892544	9	6
120	2.5462116	6	6
125	3.54025	4	6
130	5.01264	9	6
135	5.43169	14	6
140	5.91361	12	6

C. Result Tables

Table C-1: *Alpha* (for folated and non-folated micelles)

Alpha (α) ($\mu\text{m}^{-1}.\text{s}^{-1}$)		
Power Density	Folated-P105	P105
1.009	0.006003	---
1.062	0.007998	---
1.030	0.010869	0.017132
1.267	0.011178	0.015105
2.183	0.021514	0.018693
2.389	0.022303	0.025229
2.546	0.031987	0.026552
3.540	0.03972	0.040158
5.013	0.059054	0.050164
5.432	0.057413	0.049115
5.914	0.04851	0.029951

Table C-2: *Beta* for folated and non-folated micelles

Beta (β) ($\mu\text{m}^3/\text{s}$)		
Power Density	Folated-P105	P105
1.009	211.3788	---
1.062	522.4123	---
1.030	576.7294	901.8647
1.267	653.9105	772.7182
2.183	431.6908	1242.85
2.389	837.1677	1916.148
2.546	2052.618	2490.685
3.540	2171.236	2002.812
5.013	2620.417	3115.975
5.432	3601.433	3359.661
5.914	3098.037	2225.297

Table C-3: Lambda (for folated and non-folated micelles)

Lambda (λ) ($\mu\text{m}^3/\text{s}$)		
Power Density	Folated-P105	P105
1.009	258.637	---
1.062	296.937	---
1.030	355.5694	675.8224
1.267	232.174	418.6913
2.183	351.2663	345.1361
2.389	288.6013	317.2254
2.546	302.4856	319.2379
3.540	414.0641	488.7658
5.013	697.0909	611.4147
5.432	529.0142	506.0119
5.914	382.5576	329.0175

D. Release Data Graphs after Denoising:

In the following graphs, the replicates of the measurements at each power density are shown (RunX DN), together with a line representing the average of the replicates (AverageDN).

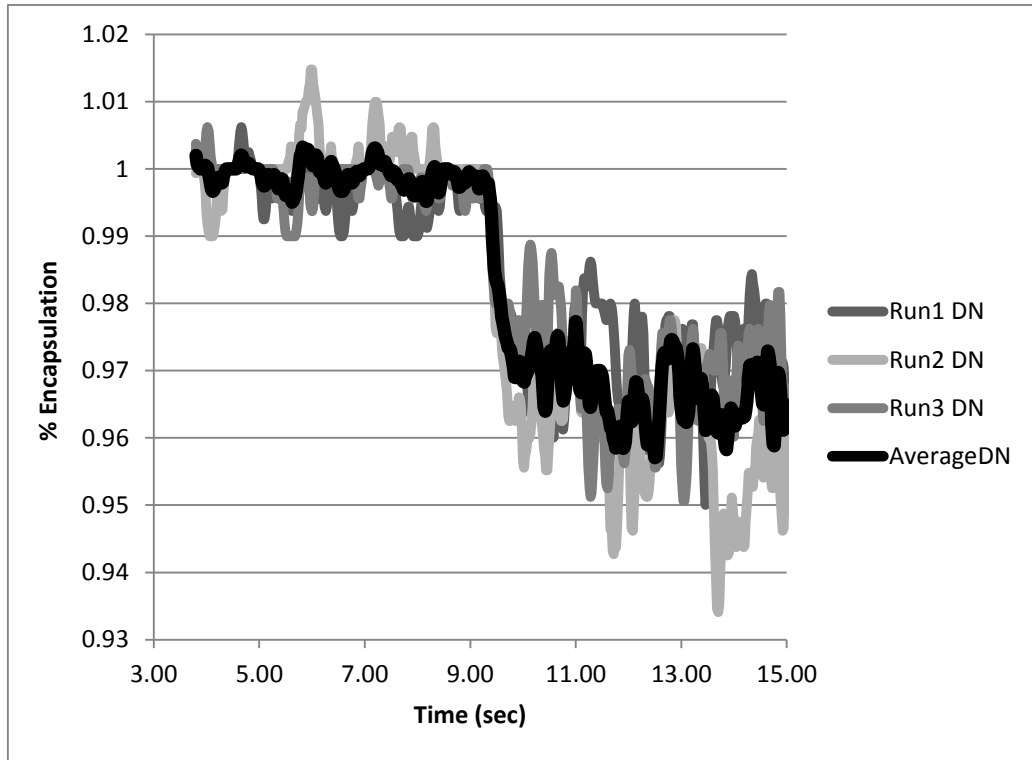


Figure D-1: Denoised release data for Folated-P105-1.009.

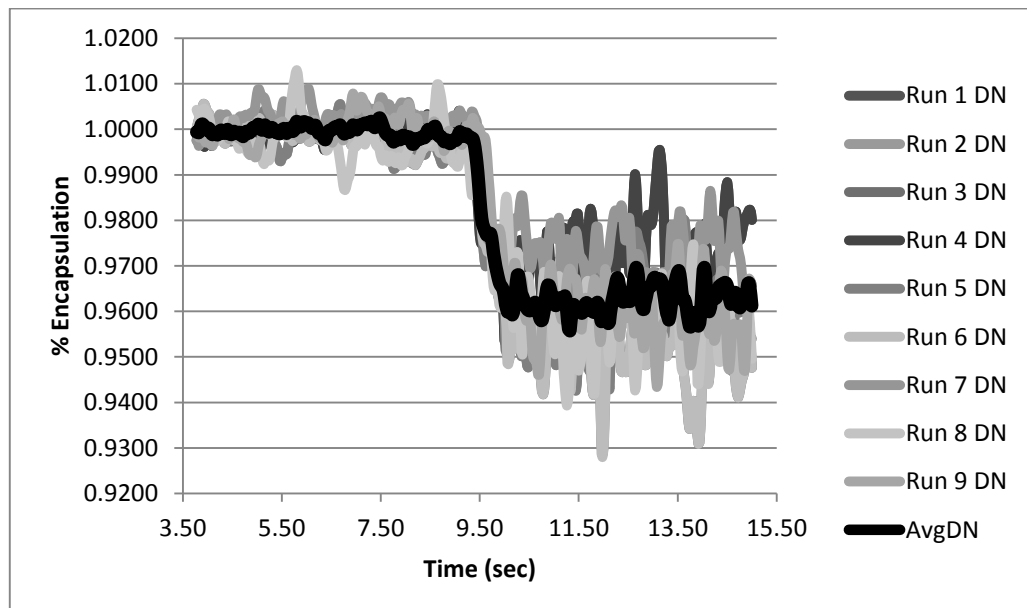


Figure D-2: Denoised release data for Folated-P105-1.062.

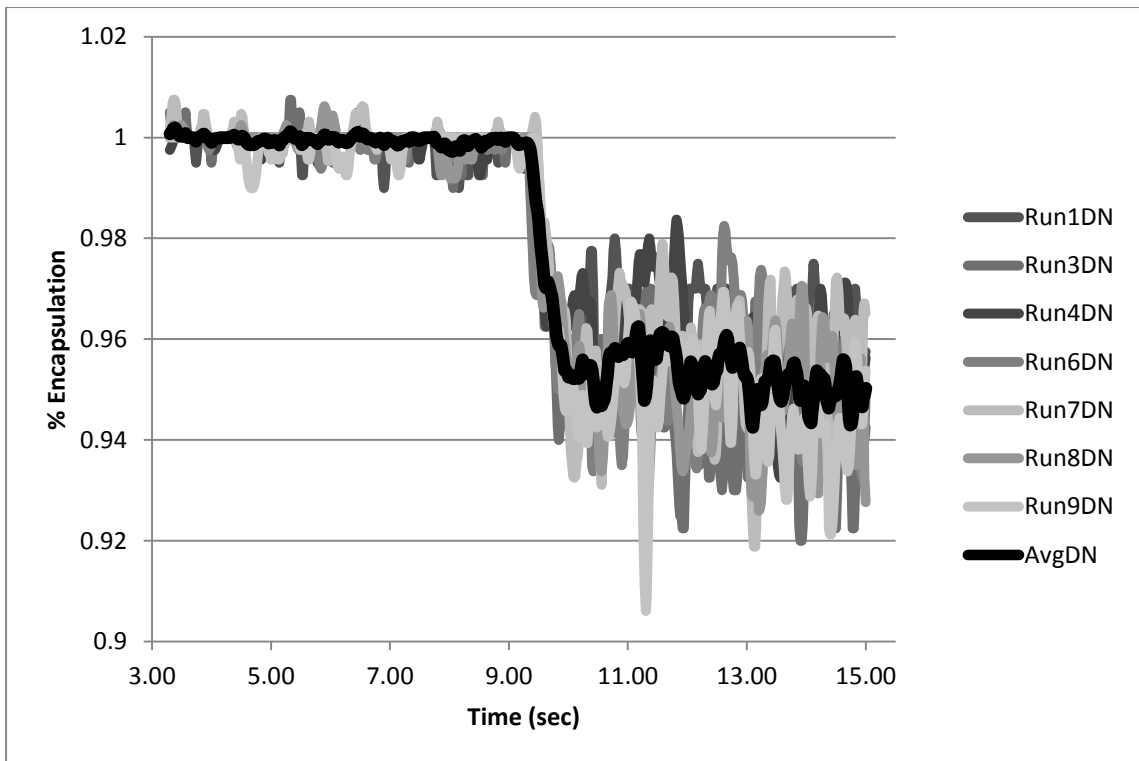


Figure D-3: Denoised release data for Folated-P105-1.030.

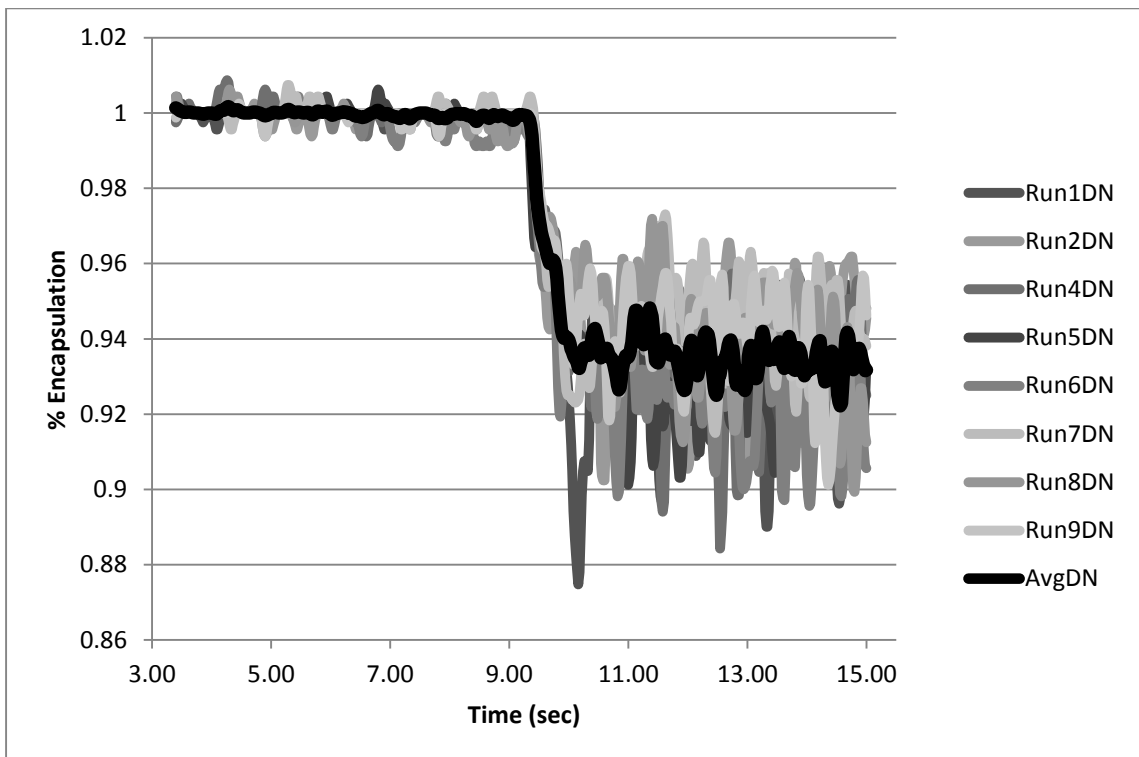


Figure D-4: Denoised release data for Folated-P105-1.267.

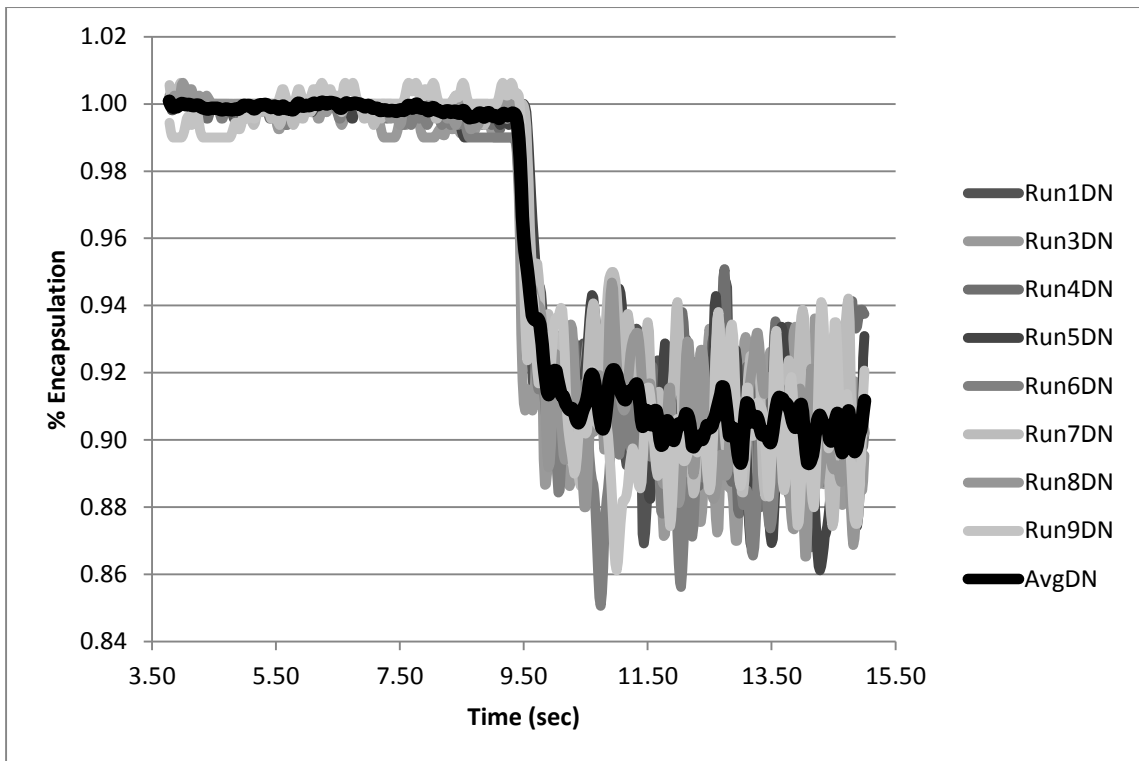


Figure D-5: Denoised release data for Folated-P105-2.183.

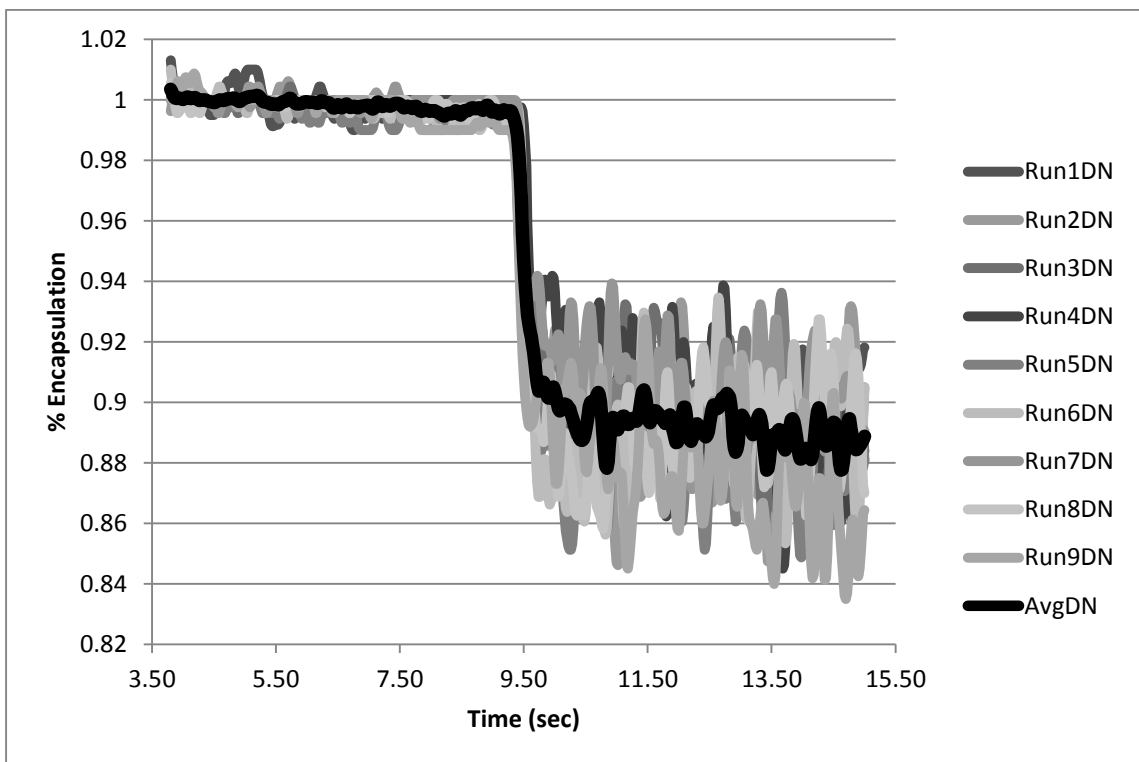


Figure D-6: Denoised release data for Folated-P105-2.389.

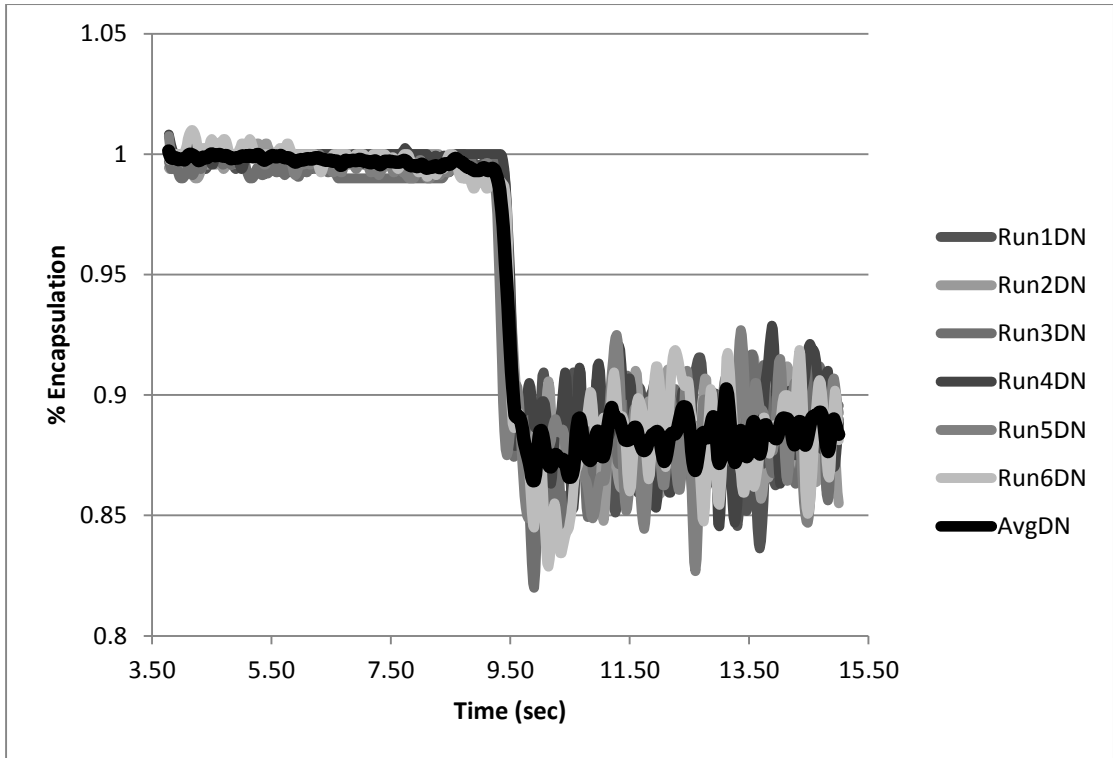


Figure D-7: Denoised release data for Folated-P105-2.546.

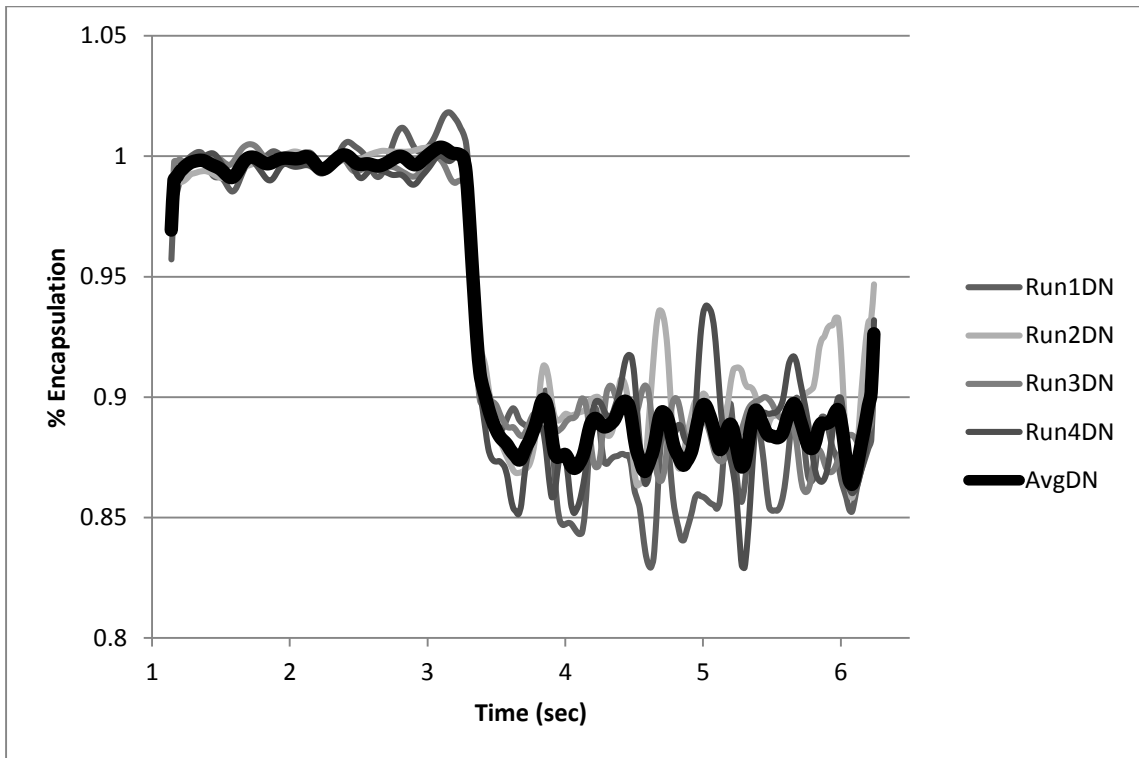


Figure D-8: Denoised Release data for Folated-P105-3.540.

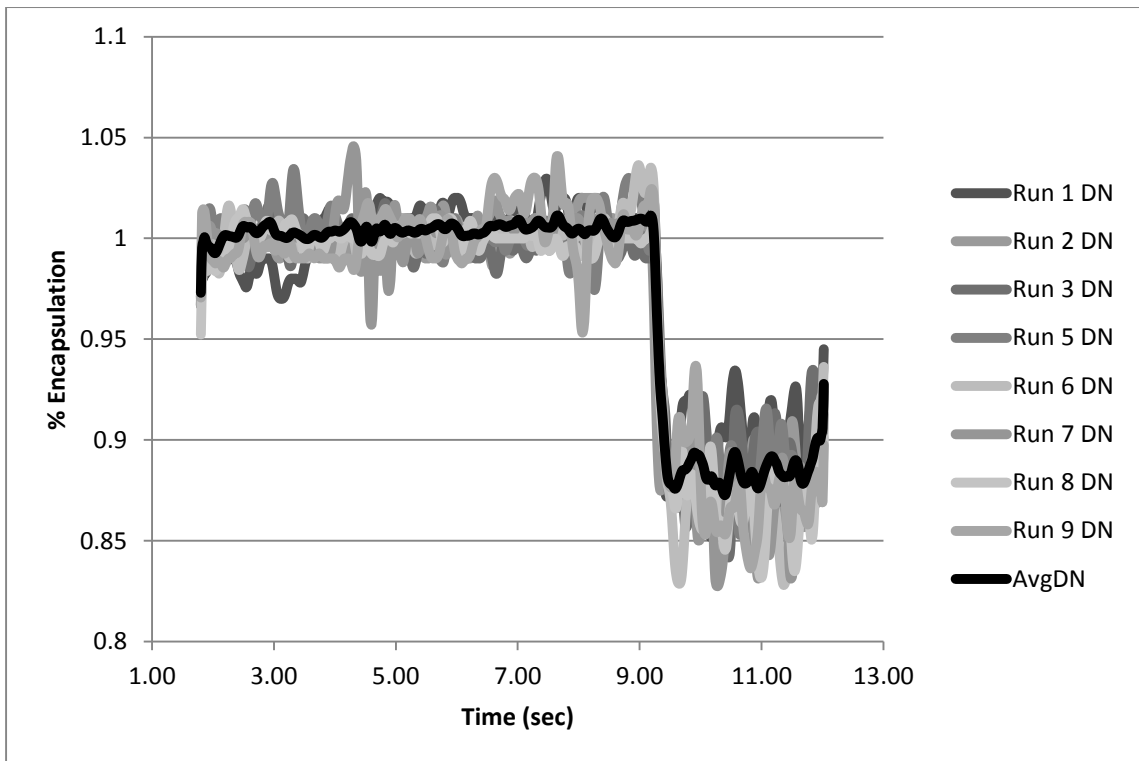


Figure D-9: Denoised release data for Folated-P105-5.013.

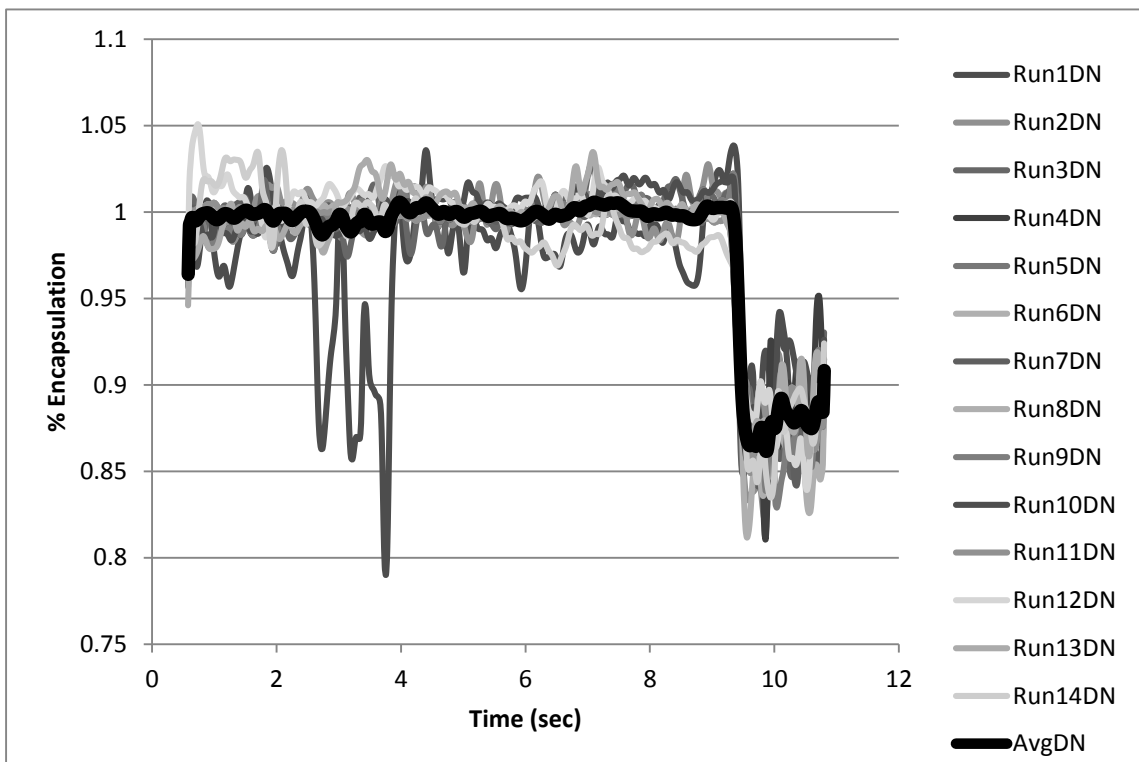


Figure D-10: Denoised release data for Folated-P105-5.432.

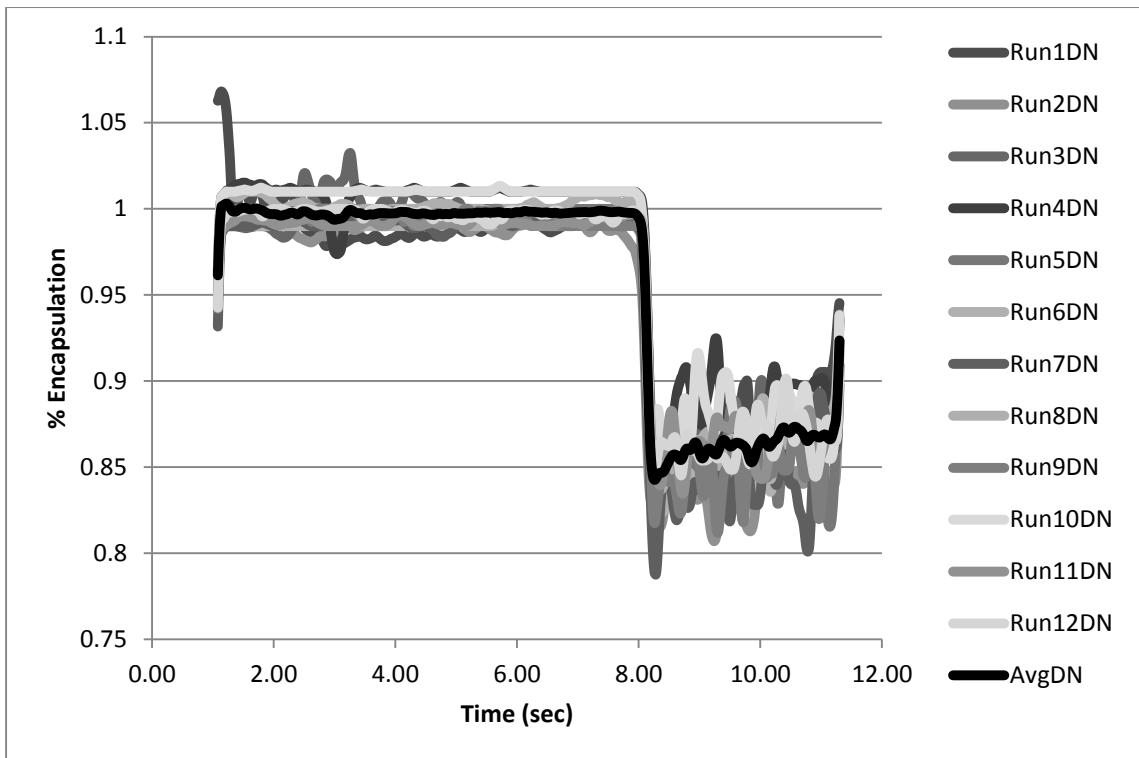


Figure D-11: Denoised release data for Folated-P105-5.914.

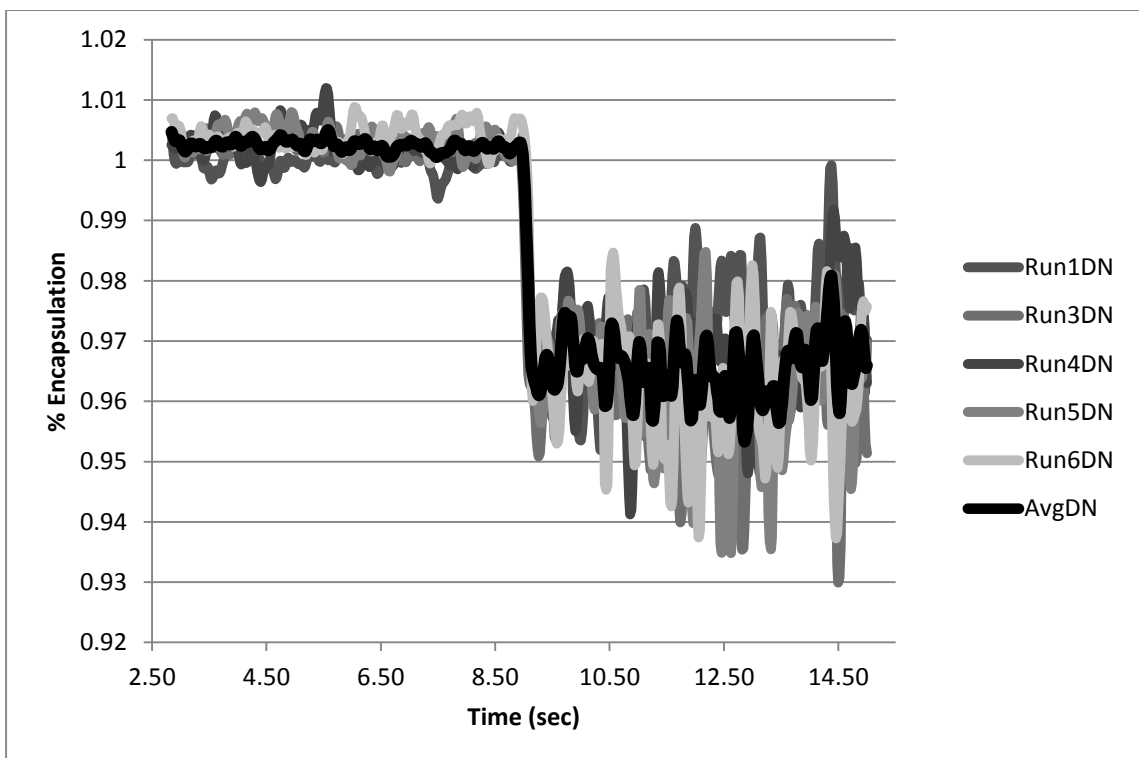


Figure D-12: Denoised release data for P105-1.030.

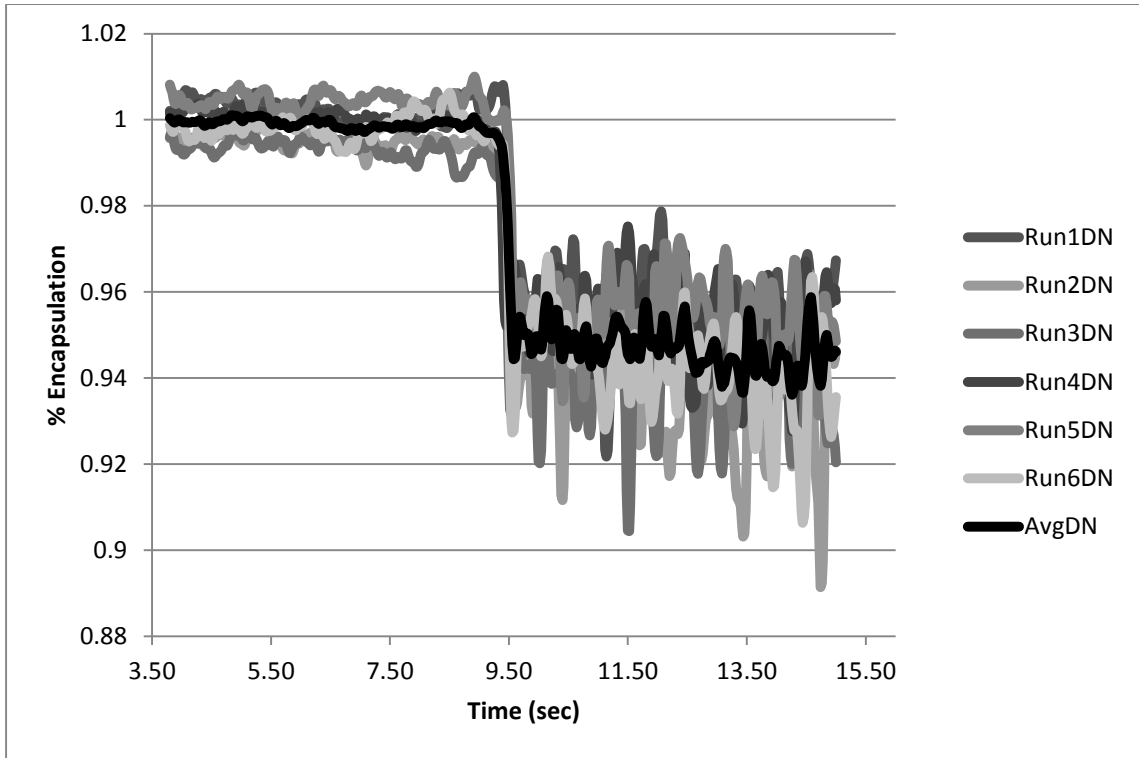


Figure D-13: Denoised release data for P105-1.267.

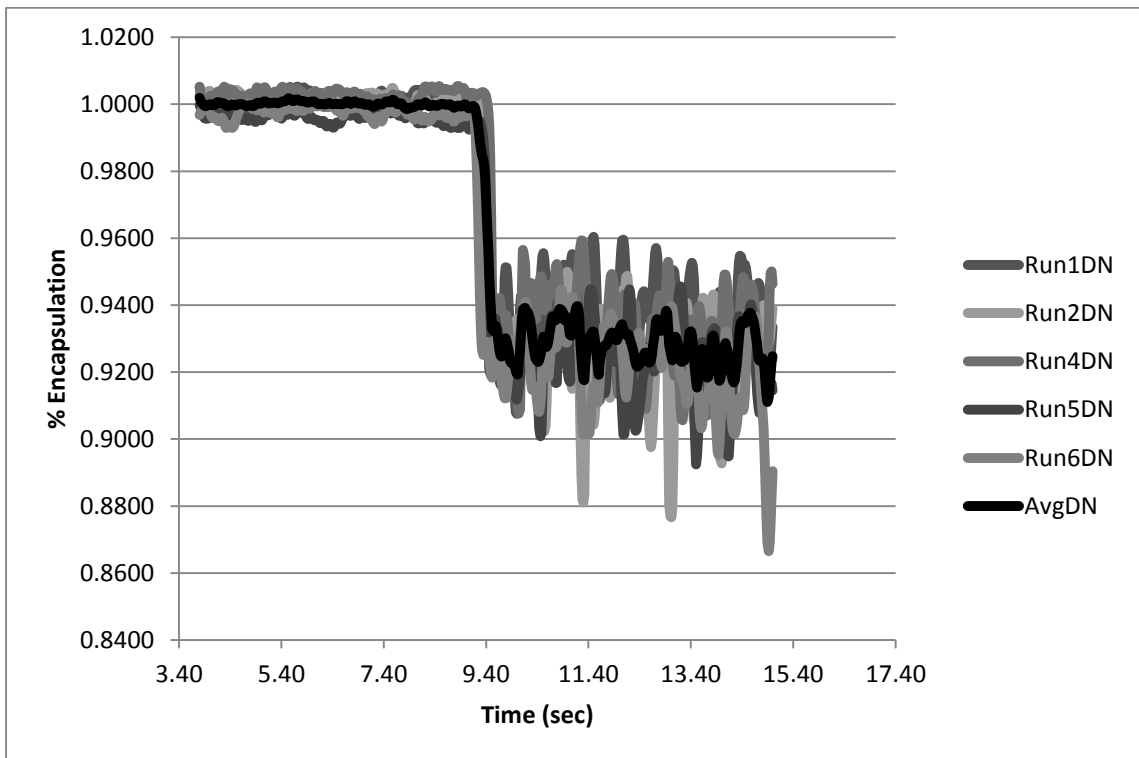


Figure D-14: Denoised release data for P105-2.183.

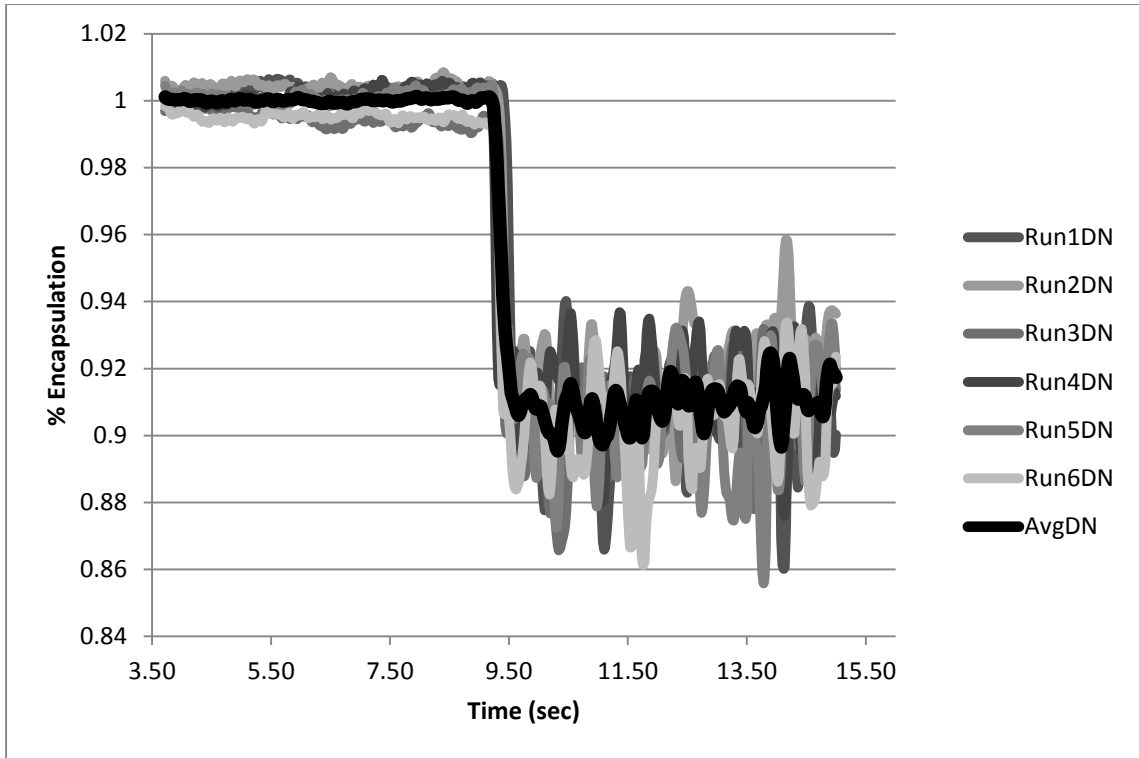


Figure D-15: Denoised release data for P105-2.389.

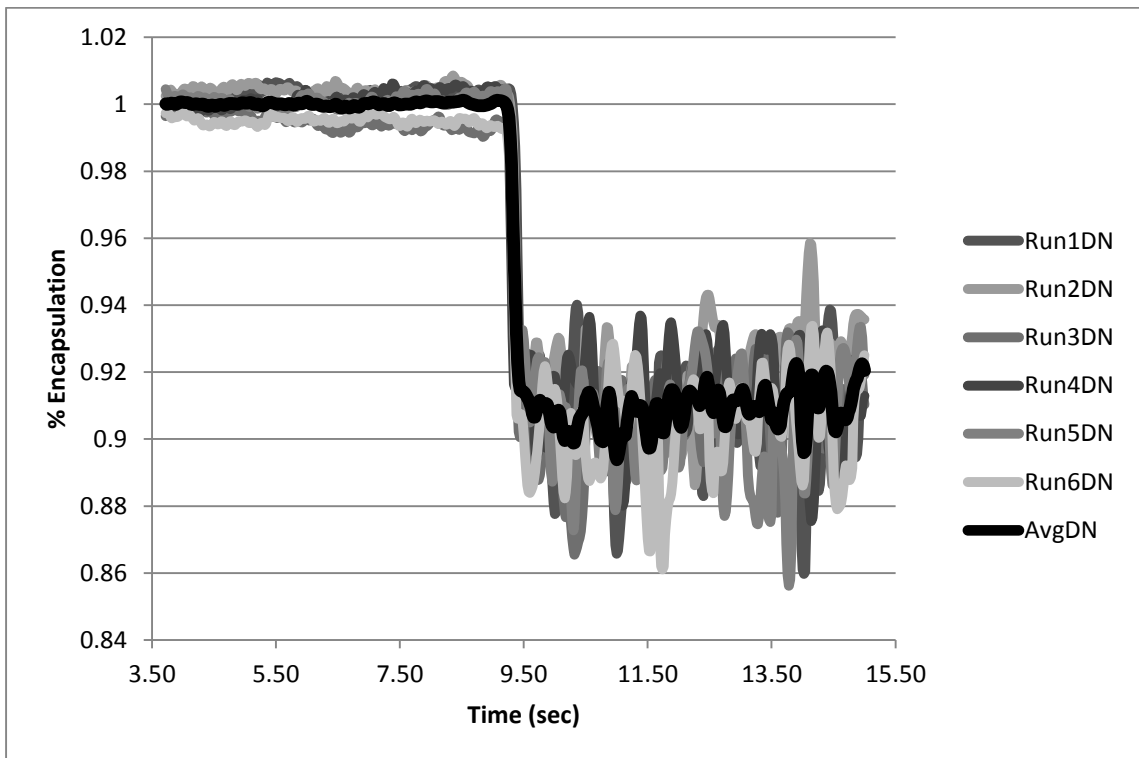


Figure D-16: Denoised release data for P105-2.546.

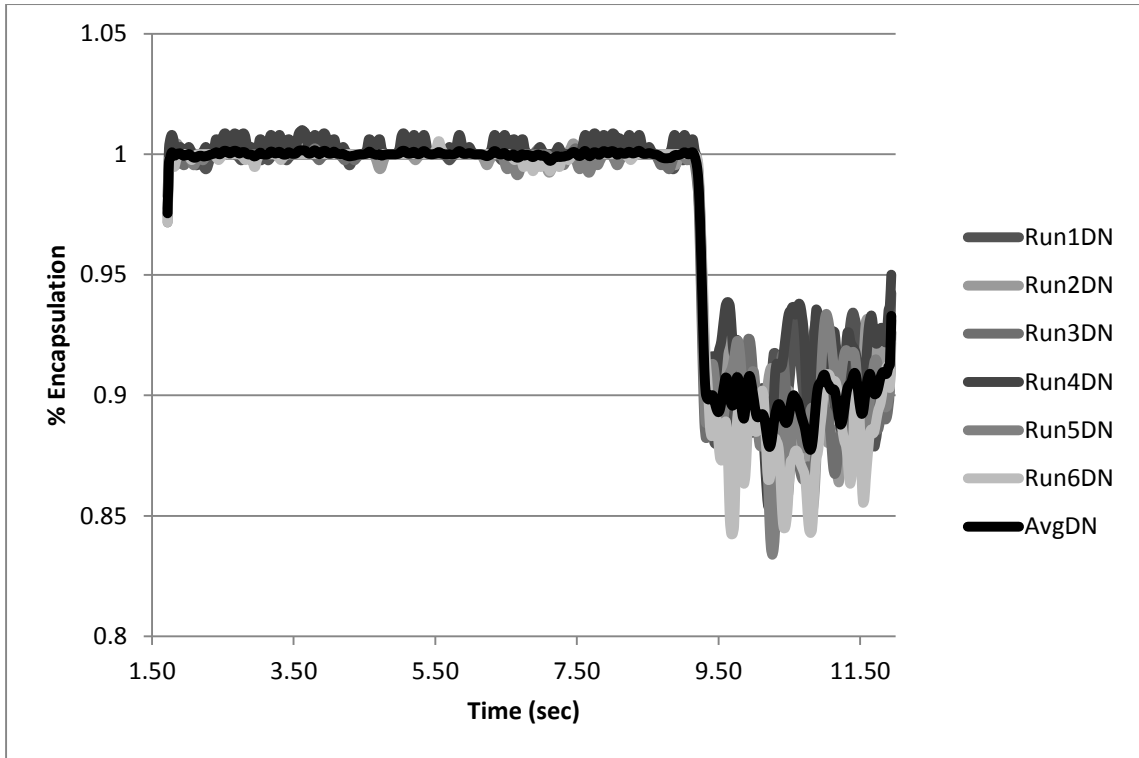


Figure D-17: Denoised release data for P105-3.540.

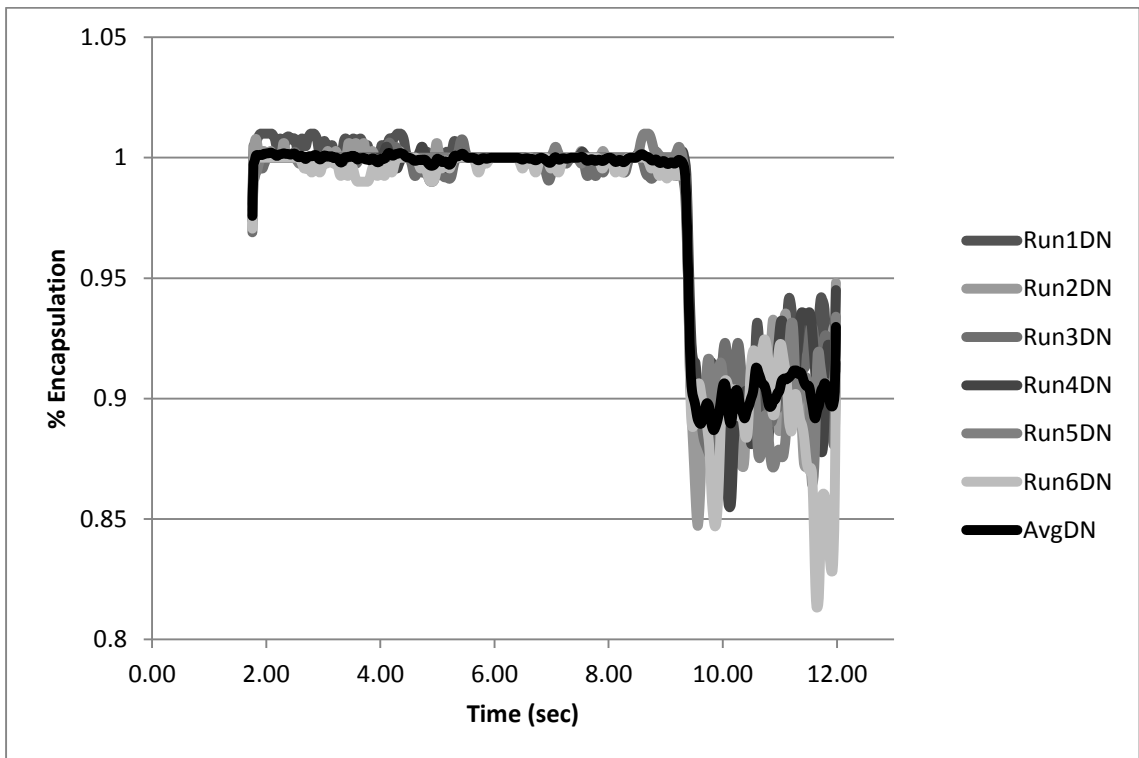


Figure D-18: Denoised release data for P105-5.013.

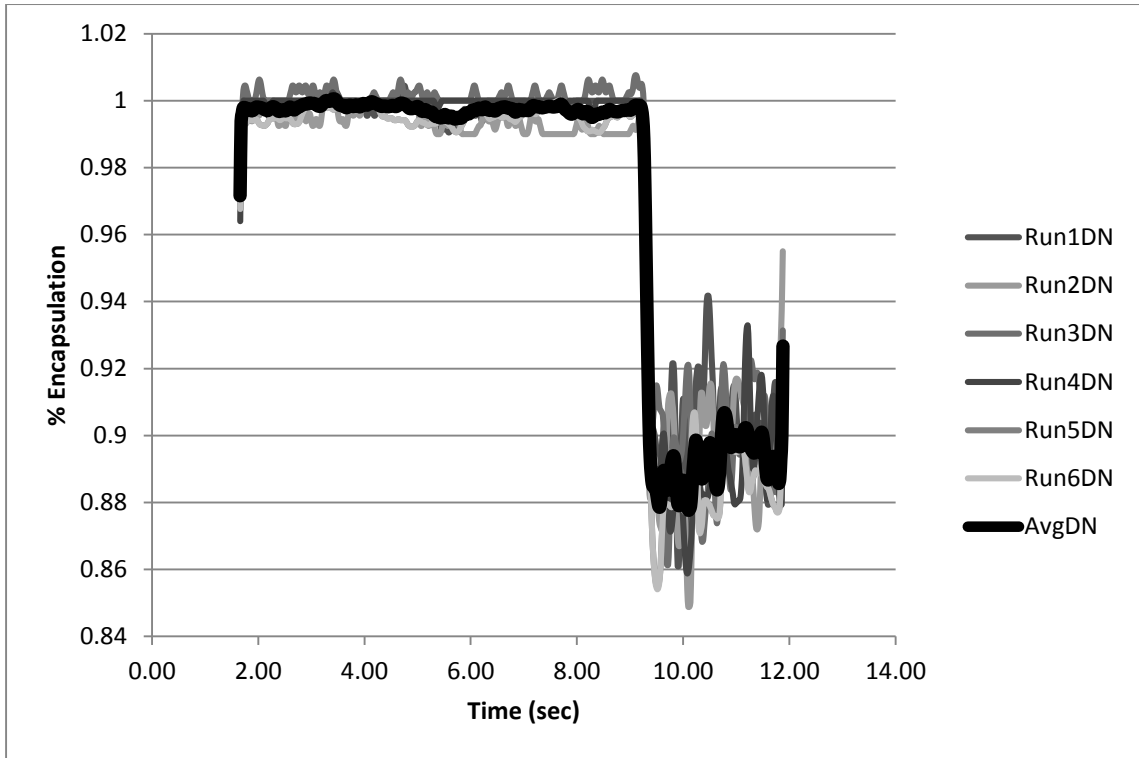


Figure D-19: Denoised release data for P105-5.432

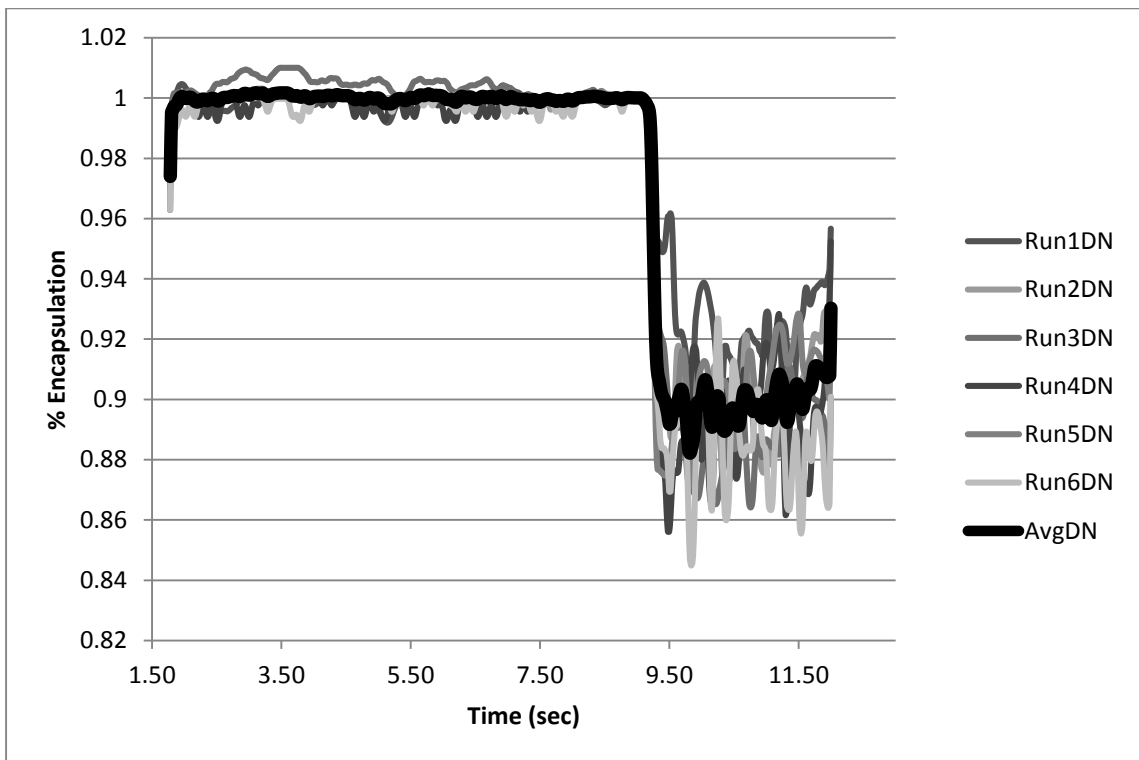


Figure D-20: Denoised release data for P105-5.914.

Vita

Rafeeq Kamal Tanbour was born on April 15, 1988, in Nablus, Palestine. He received his high school diploma from Islamic Secondary School in Nablus, in 2006. He then moved to An-Najah National University in Nablus, from which he graduated, in 2012. His degree was a Bachelor's of Chemical Engineering. Mr. Tanbour then moved to the United Arab Emirates in 2013 and began a Master's program in Chemical Engineering at the American University of Sharjah.

Mr. Tanbour is worked during his master study as a teaching assistant. Also he is a member of the Jordanian Engineering Association.